

# Challenges and Perspectives for NASICON-Type Electrode Materials for Advanced Sodium-Ion Batteries

Shuangqiang Chen, Chao Wu, Laifa Shen, Changbao Zhu, Yuanye Huang, Kai Xi, Joachim Maier, and Yan Yu\*

Sodium-ion batteries (SIBs) have attracted increasing attention in the past decades, because of high overall abundance of precursors, their even geographical distribution, and low cost. Apart from inherent thermodynamic disadvantages, SIBs have to overcome multiple kinetic problems, such as fast capacity decay, low rate capacities and low Coulombic efficiencies. A special case is sodium super ion conductor (NASICON)-based electrode materials as they exhibit – besides pronounced structural stability – exceptionally high ion conductivity, rendering them most promising for sodium storage. Owing to the limiting, comparatively low electronic conductivity, nano-structuring is a prerequisite for achieving satisfactory rate-capability. In this review, we analyze advantages and disadvantages of NASICON-type electrode materials and highlight electrode structure design principles for obtaining the desired electrochemical performance. Moreover, we give an overview of recent approaches to enhance electrical conductivity and structural stability of cathode and anode materials based on NASICON structure. We believe that this review provides a pertinent insight into relevant design principles and inspires further research in this respect.

due to advantages in terms of energy capacity ( $\approx 100\text{--}300 \text{ Wh kg}^{-1}$ ) and volume density ( $\approx 250\text{--}650 \text{ Wh L}^{-1}$ ).<sup>[1\text{--}6]</sup> Now, with LIBs entering the fields of large-scale energy storage devices in particular for grid storage, they face severe bottle-necks owing to limited energy densities, low lithium abundance and relatively high cost.<sup>[4,7\text{--}11]</sup> Compared to LIBs, sodium-ion batteries (SIBs) offer multiple advantages such as abundancy of elemental source, evenly geographical distribution and distinctly lower cost are hence recognized as serious alternative to LIB.<sup>[7,12\text{--}17]</sup> The application potential of SIB is indeed expected to be competitive with LIB systems, not so much in terms of thermodynamic, but rather in terms of kinetic criteria.<sup>[18,19]</sup> In some cases, Na-ion batteries have even been shown better electrochemical performance than Li-ion batteries.<sup>[20,21]</sup>

At a first glance, the different position of Na in the periodic system when compared to Li predicts serious disadvantages. The ionic radius is larger (1.02 Å vs 0.76 Å) and the weight heavier (23 g mol<sup>-1</sup> vs 7 g mol<sup>-1</sup>) as a consequence of which one expects worse transport kinetics, lower solubility in the solid state, less favorable gravimetric and volumetric figures of merit and lower Madelung energies, giving rise to low cell voltages. Insertion/desertion of Na<sup>+</sup> ions into most host materials, including sodium oxides (NaMO<sub>2</sub>, M = V, Fe, Mn, Cu, Co, and Ni), transition metal fluorides (NaMF<sub>3</sub>; M = Fe, Mn, Ni and V), sodium phosphates (Na<sub>7</sub>V<sub>3</sub>(P<sub>2</sub>O<sub>7</sub>)<sub>4</sub>, NaFePO<sub>4</sub>) and transition metal oxides (V<sub>2</sub>O<sub>5</sub>)<sup>[22\text{--}37]</sup> are worse than for Li-analogues. In spite of these disadvantages, the “extrinsic” advantages of SIBs make them attractive nonetheless.

At a second glance, the apparent “intrinsic” disadvantages have to be estimated more subtly: Electro-positivity of sodium is higher and polarizability of the ion as well. As a consequence, the cell potential using Li-analogues is not necessarily larger, even though this is correct for most systems. More importantly, the increased ionic radius has two decisive advantages: One is that the solvation in liquid electrolytes is less severe than for the highly polarizing small lithium ion and thus the transfer resistance caused by bringing the ions from the liquid electrolyte into the electrode is typically smaller. More importantly, the higher ionic radius enables solid structures with enormous ion conductivities that are not realizable with Li. A classic example

## 1. Introduction

In the last two decades, lithium ion batteries (LIBs) have been found widely spread applications mostly in the fields of energy and information conversion, but also for actuation. They proved extremely worthwhile for various applications, such as portable smart devices, electric vehicles or robots. This is essentially

Prof. Y. Yu  
Key Laboratory of Materials for Energy Conversion  
Chinese Academy of Sciences  
Department of Materials Science and Engineering  
University of Science and Technology of China  
Hefei, Anhui 230026, China  
E-mail: yanyumse@ustc.edu.cn

Dr. S. Chen, Dr. C. Wu, Dr. L. Shen, Dr. C. Zhu, Msc. Y. Huang,  
Prof. Dr. J. Maier, Prof. Dr. Y. Yu  
Max Planck Institute for Solid State Research  
Heisenbergstrasse 1, 70569 Stuttgart, Germany  
Dr. K. Xi  
Department of Materials Science & Metallurgy  
University of Cambridge  
27 Charles Babbage Road, Cambridge CB3 0FS, UK

The ORCID identification number(s) for the author(s) of this article can be found under <https://doi.org/10.1002/adma.201700431>.

DOI: 10.1002/adma.201700431

is the  $\beta$ -aluminas for which the sodium ion is of perfect size and polarizability. Similarly, in the sodium super ionic conductor (NASICON) family, sodium ion conductivities can be very high and exceed Li-ion conductivities by far. Moreover, the flexibility of the NASICON structure allows also the accommodation of transition metal ions, by which electronic conductivity is induced and Na-storage is enabled.

In spite of the so-induced mixed conductivity, NASICON based electrode materials show insufficient chemical diffusion owing to the limited electronic conductivity and the tools of nanotechnology have to be applied to improve performance. In addition to particle size reduction, coating by a medium that conducts electrons but does not prevent ionic access (e.g., doped carbon materials) is the procedure of choice.<sup>[38–41]</sup>

Present SIBs anodes can be divided into five main categories: 1) metals and alloys (Na, Sn, Sb, Ge, Sn-Ge and Sn-Ge-Sb);<sup>[16,42–47]</sup> 2) carbon based materials (porous hard carbon, nitrogen-doped carbon nanofibers);<sup>[12,48–51]</sup> 3) non-metallic elements (P, and S);<sup>[14,52–55]</sup> 4) metal oxides/sulphides/selenides/phosphides ( $TiO_2$ ,  $SnO_2$ ,  $CoSe_2$ ,  $CoSe$ ,  $Sb_2O_4$ ,  $Sb_2S_3$ ,  $SnS_2$ ,  $WS_2$ ,  $MoS_2$ , and  $NiP_3$ );<sup>[17,56–68]</sup> and last but not least 5) NASICON based materials ( $NaTi_2(PO_4)_3$ ).<sup>[69–71]</sup> The corresponding voltages and capacities of cathode and anode materials for SIBs are summarized in Figure 1a.

## 2. Components of Sodium-Ion Batteries

Typical SIBs use, as LIBs, the rocking chair principle,<sup>[13,72–75]</sup> and are composed of four components, namely positive electrode, negative electrode, separator and non-aqueous salt containing electrolyte. The typical SIB shown in Figure 1b uses 1M  $NaClO_4$  containing propylene carbonate/ethylene carbonate as electrolyte. During the charging process,  $Na^+$  ions leave typical cathode such as  $Na_3V_2(PO_4)_3$  or layered  $NaCoO_2$ , and are incorporated in the anode while the electrons flows via the external circuit from the positive electrode to the negative electrode. During discharging, the process is reversed. One very important advantage of SIBs, shown in Figure 1b, is reflected on cost control. One can apply commercial aluminum foil as current collector for both cathode and anode, while Cu is necessary on the negative side of LIBs (Al alloys with Li but not with Na). The price of Al foil (\$70 per 100 m, battery grade) is a third of the price of copper foil (\$210 per 100 m, battery grade),<sup>[76]</sup> which significantly reduces the overall battery cost.

In this review, we focus on NASICON electrode materials, the major advantages of which, namely high ionic conductivity and structural stability, have already been mentioned. The list should be complemented by chemical flexibility and thermal stability. The general formula of NASICON materials can be given as  $Na_xMM'(XO_4)_3$  ( $M = V, Ti, Fe, Tr$  or  $Nb$  etc.;  $X = P$ , or  $S$ ,  $x = 0–4$ ). The NASICON framework structure is constructed by corner-shared  $MO_6$  ( $M' O_6$ ) and polyhedral  $XO_4$  groups, providing pronounced  $Na^+$  diffusion channels.<sup>[77]</sup> As cathodes  $Na_3V_2(PO_4)_3$ ,  $Na_3V_2(PO_4)_2F_3$ ,  $Na_{1.5}VPO_4F_{0.5}$ ,  $Na_2FeTi(PO_4)_3$ , and  $Fe_2(MoO_4)_3$  have been particularly well investigated.<sup>[78–80]</sup> NASICON materials with low redox potential are  $NaTi_2(PO_4)_3$ ,  $NaZr_2(PO_4)_3$ ,  $NaV_2(PO_4)_3$ , and  $Na_3MnTi(PO_4)_3$ ; they can serve as anodes.



**Shuangqiang Chen** completed his Ph.D. study in December 2014 at University of Technology Sydney (UTS). He worked as a Research Associate at the Center for Clean Energy Technology in UTS in 2015. He is currently working as an Alexander von Humboldt Research Fellow at the Max Planck Institute for Solid State Research, directed by Prof. Yu and Prof. Maier since 09/2015. His research mainly focuses on the synthesis of novel, porous and functional nanocomposites and the applications of energy storage and electrochemical catalysis, including Li-ion batteries, Li-S batteries,  $Li-O_2$  batteries, Na-ion batteries, and electrochemical water splitting.



**Joachim Maier** is a director at the Max Planck Institute for Solid State Research in Stuttgart (Germany) and heads the department of Physical Chemistry J. Maier studied chemistry in Saarbrücken, and obtained his Masters and PhD in Physical Chemistry there. He completed his professorial thesis (Habilitation) at the University of Tübingen. From 1988 to 1991 he was responsible for the activities on functional ceramics at the MPI for Metals Research in Stuttgart, and from 1988 to 1996 (as a Foreign Faculty Member) he taught defect chemistry at the Massachusetts Institute of Technology. In 1991, he was appointed Scientific Member of the Max Planck Society, Director at the MPI for Solid State Research and Honorary Professor at the University of Stuttgart.



**Yan Yu** is working in University of Science and Technology of China (USTC). She received her Ph.D. in material science at USTC in 2006. From 2007 to 2008, she worked as a postdoctoral at Florida International University. After that she received Humboldt Research Fellowship and the Sofja Kovalevskaja award from the Alexander von Humboldt Foundation and worked at the Max Planck Institute for Solid State Research in Stuttgart, Germany. Her current research interests mainly include design of novel nanomaterials for clean energy, especially for batteries and the fundamental science of energy storage system.

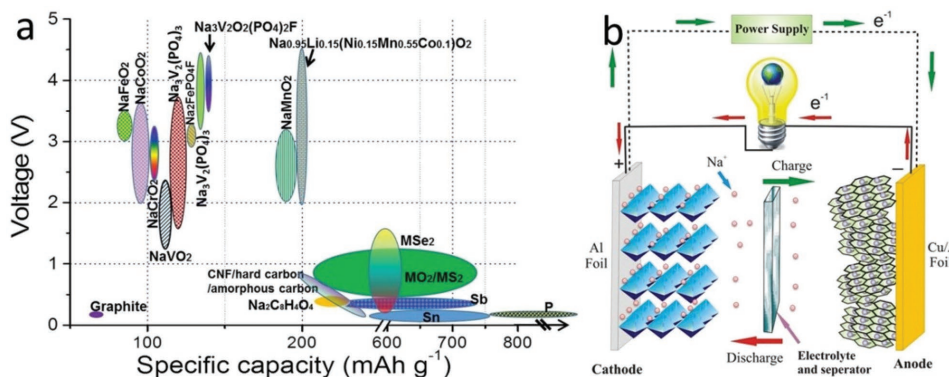


**Figure 1.** a) Typical cathode and anode materials for SIBs: represented by their voltages and specific capacities with sodium foils as counter electrodes. b) Schematics of a sodium ion battery.

For instance,  $\text{NaTi}_2(\text{PO}_4)_3$  based on  $\text{Ti}^{3+}/\text{Ti}^{4+}$  conversion exhibits a discharge voltage at 2.1 V and a reversible capacity of 120  $\text{mAh g}^{-1}$ ,<sup>[69]</sup> and is considered as anode material.  $\text{Na}_3\text{V}_2(\text{PO}_4)_3$  based on the redox conversion of  $\text{V}^{3+}/\text{V}^{4+}$  displays a discharge voltage of 3.4 V, serving as cathode materials with a capacity of 117  $\text{mAh g}^{-1}$ , while the redox conversion of  $\text{V}^{2+}/\text{V}^{3+}$  provides a low voltage of 1.6 V, leading to an anode material with a capacity of 50  $\text{mAh g}^{-1}$ .<sup>[81,82]</sup>

## 2.1. The Storage Kinetics of NASICON Materials

The ionic conductivity has been thoroughly measured and structurally analyzed for NASICON solid electrolytes, mainly in the 1980s and 1990s. Detailed material science of NASICON started with the seminal work by Hong, Goodenough and Kafalas.<sup>[83,84]</sup> In particular, for the  $\text{Na}_{1+x}\text{Zr}_x\text{Si}_x\text{P}_{3-x}\text{O}_{12}$  materials, enormous Na-ion conductivities have been measured and the conductivity mechanisms explored. It was also soon recognized that also transition metal elements can be implanted in the structure. For details, the reader is referred to the extensive literatures.<sup>[85–89]</sup> In particular, ref. [89] gives a very detailed report, not only on the ion conductivity mechanisms, but also on phase thermodynamics, thermodynamic and kinetic stability of the solid electrolyte materials with respect to sodium.

It is shown that thermodynamic stability against Na requires absence of phosphate which already leads to a much lower conductivity.<sup>[90]</sup> This does not rule out NASICON's use as solid electrolyte if lower temperature is considered and passivation layers are formed. In this contribution, however we concentrate on the use of electrodes. Nonetheless, the ion transport issues clarified in the electrolyte literatures form the basis for the ion transport in the NASICON electrode as well.<sup>[91–93]</sup>

The discussion of storage kinetics is non-trivial, and it is not solely transport controlled. This is not only due to the heterogeneity of the situation but also due to the super-position of migration and diffusion. The situation can be grossly simplified if the electrode is either predominately ionically or electronically conductive, which is normally the case. Given sufficiently fast access of ions (liquid electrolyte) and electrons (current collecting phase) to the electroactive particles (including fast phase transfer), the storage kinetics is then a chemical

diffusion problem, whereby the chemical diffusion coefficient is given by<sup>[94]</sup>

$$D^\delta \propto \frac{\sigma_{\text{ion}} * \sigma_{\text{eon}}}{\sigma} \left( \frac{\chi_{\text{eon}}}{c_{\text{eon}}} + \frac{\chi_{\text{ion}}}{c_{\text{ion}}} \right) \quad (1)$$

$c_{\text{eon}}$  and  $c_{\text{ion}}$  are the concentration of the electronic and ionic carriers. The  $\chi$ -factors describe internal trapping reactions, which are usually crucial at the temperature of operation. If we assume  $\sigma_{\text{ion}} \gg \sigma_{\text{eon}}$  and  $c_{\text{ion}} \gg c_{\text{eon}}$  for our NASICON materials,<sup>[95]</sup>

$$D^\delta \propto \chi_{\text{eon}} D_{\text{eon}} \quad (2)$$

Showing that  $D^\delta$  is determined by the electronic mobility (proportional to  $D_{\text{eon}}$ ) and trapping reactions ( $\chi$  factors). The second part of the transport kinetics is the conduction of electrons and ions to the particles. In the case of porous morphologies and liquid electrolytes, it is essentially the transport of electrons that is decisive, more so since the ion conductivity of NASICON particles assists in ion percolation. Typical values of chemical diffusion coefficients are listed in Table 1 along with references.<sup>[96–98]</sup> Unfortunately, literature values are often not reliably measured bulk values but influenced by issues of size, interfaces or phase transformations), and thus are essential effective values ( $D^\delta$  values have been reliably on single crystalline  $\text{LiFePO}_4$  ( $1.6 \times 10^{-9} \text{ cm}^2 \text{ s}^{-1}$  but at 150 °C).<sup>[99]</sup> Overall it appears that NASICON structures provide values around  $10^{-10} \text{ cm}^2 \text{ s}^{-1}$  exceeding values of most other electrode phases.

As the electronic conductivity of NASICON materials is poor, electronic wiring by adding current collecting phases such as carbon and additional conductive coating e.g., by deliberate carbon coating is important. Figure 2a–b shows the typical solutions used in literatures. As far as the transport kinetics in the electroactive particles is concerned, there are essentially two adjusting screws as obvious from the relaxation time<sup>[95]</sup>

$$\tau^\delta \propto L^2 / D^\delta \quad (3)$$

in which  $\tau$  stands for duration of chemical diffusion,  $D$  is chemical diffusion coefficient and  $L$  is the diffusion length (regarding to the whole length of a bulk electrode). The first is  $D^\delta$ , which cannot be greatly influenced. Doping mostly helps

**Table 1.** Effective diffusion coefficient (EDC) in literature (the following abbreviations are used: Room temperature (RT), ethylene carbonate (EC), propylene carbonate (PC), dimethyl carbonate (DMC), diethyl carbonate (DEC), fluoroethylene carbonate (FEC), polyethylene glycol methyl ether methacrylate (PEGMA), bisphenol A ethoxylate dimethacrylate (BEMA), dimethylsulfoxide (DMSO); Galvanostatic intermittent titration technique (GITT), cyclic voltammetry (CV), potentiostatic intermittent titration technique (PITT), electrochemical impedance spectroscopy (EIS)).

Materials	EDC ( $\text{cm}^2 \text{S}^{-1}$ )	Test environment	Test technique	Ref.
$\text{LiFePO}_4$ ; $\text{FePO}_4$	$1.8 \times 10^{-14}, 2.2 \times 10^{-16}$	20 °C; 1 M $\text{LiPF}_6$ in EC/DMC	GITT	[100]
Carbon fiber	$\approx 10^{-10}$	20 °C; 1 M $\text{LiPF}_6$ in EC/DMC	CV	[101]
Graphite	$1.12 \times 10^{-10}, 1.35 \times 10^{-10}$ (55 °C)	20 °C; 1 M $\text{LiPF}_6$ in EC/DMC	PITT	[102]
Graphene (Bilayer)	$10^{-6} \approx 7 \times 10^{-5}$	RT; 0.35 M LiTFSI in PEGMA:BEMA (3:7) and 2 ≈ 4% 2-hydroxy-2-methylpropiophenone	in situ time-resolved Hall measurement	[103]
$\text{Li}_3\text{V}_2(\text{PO}_4)_3$	$\approx 10^{-11} - 10^{-9}$ (Single phase); $\approx 10^{-10}$ (Two phase, $\approx 10^{-12}$ at 2 V)	20 °C; 1 M $\text{LiPF}_6$ in EC/DMC (1:1, w/w)	GITT	[104]
$\text{NaNi}_{0.5}\text{Mn}_{0.5}\text{O}_2$ ; $\text{LiNi}_{0.5}\text{Mn}_{0.5}\text{O}_2$	$7.7 \times 10^{-12}, 6 \times 10^{-13}$	25 °C; 0.5 M $\text{NaPF}_6$ in PC with 2 wt.% FEC; 0.5 M $\text{LiPF}_6$ in PC/FEC (98:2; w/w)	EIS	[105]
$\text{Na}_{0.9}\text{FePO}_4$ ; $\text{Li}_{0.9}\text{FePO}_4$	$8.63 \times 10^{-17}, 6.77 \times 10^{-16}$	25 °C; $\text{NaClO}_4$ in EC/DMC (1:1; v/v); $\text{LiPF}_6$ in EC/DEC (1:1; v/v)	GITT	[97]
$\text{P2-Na}_{2/3}[\text{Ni}_{1/3}\text{Mn}_{2/3}]\text{O}_2$	$7 \times 10^{-9} \approx 1 \times 10^{-10}$ (Na); $3 \times 10^{-9} \approx 2 \times 10^{-11}$ (Li)	25 °C; $\text{NaPF}_6$ in EC/DEC (1:2; v/v); $\text{LiPF}_6$ in EC/DEC (1:1; v/v)	GITT	[106]
$\text{P2-Na}_{0.62}\text{Ti}_{0.37}\text{Cr}_{0.63}\text{O}_2$	$1 \times 10^{-12} \approx 2 \times 10^{-13}$	25 °C; $\text{NaClO}_4$ in PC with 2 vol.% FEC	GITT	[98]
$\text{Na}_{0.44}\text{MnO}_2$	$5.75 \times 10^{-16} \approx 2.14 \times 10^{-14}$	25 °C; $\text{NaClO}_4$ in EC/DMC (1:2; v/v)	EIS	[96]
$\text{NaSn}_2(\text{PO}_4)_3$ (NASICON)	$6.03 \times 10^{-12}$	25 °C	GITT	[107]
$\text{Na}_3\text{V}_2(\text{PO}_4)_3@\text{C/G}$ (NASICON)	$4.59 \times 10^{-10} \approx 1.99 \times 10^{-9}$	25 °C; 1 M $\text{NaClO}_4$ in EC/DEC (1:2; v/v) with 2 vol.% FEC	EIS	[108]
$\text{Na}_3\text{V}_2(\text{PO}_4)_3\text{-C}$ (NASICON)	$2 \times 10^{-15} \approx 6 \times 10^{-13}$	25 °C; $\text{NaPF}_6$ in PC	GITT	[109]
$\text{Na}_3\text{V}_2(\text{PO}_4)_3@\text{C-B-doped}$ (NASICON)	$4.0 \times 10^{-14} \approx 2.48 \times 10^{-13}$	RT; 0.8 M $\text{NaClO}_4$ in EC/DEC (1:1; v/v)	EIS	[110]
$\text{NaTi}_2(\text{PO}_4)_3$ (NASICON)	$2.0 \times 10^{-13}$	RT; 1 M $\text{NaClO}_4$ in EC/DEC (1:1; v/v) with 3 wt.% FEC	EIS	[111]
$\text{NaTi}_2(\text{PO}_4)_3@\text{C}$ (NASICON)	$1.79 \approx 2.32 \times 10^{-10}$	RT; 1 M $\text{NaClO}_4$ in EC/PC (1:1; v/v)	CV	[112]
$\text{NaTi}_2(\text{PO}_4)_3$ thin film (NASICON)	$\ast 10^{-9} \approx 10^{-12}$	RT; 1 M $\text{NaCF}_3\text{SO}_3$ in DMSO	GITT	[113]
$\text{Na}_{3.1}\text{Zr}_{1.95}\text{Mg}_{0.05}\text{Si}_2\text{PO}_{12}$ (Electrolyte, NASICON)	$5.24 \times 10^{-8}$	RT; solid electrolyte ( $\text{Na}_{3.1}\text{Zr}_{1.95}\text{Mg}_{0.05}\text{Si}_2\text{PO}_{12}$ )	CV	[114]

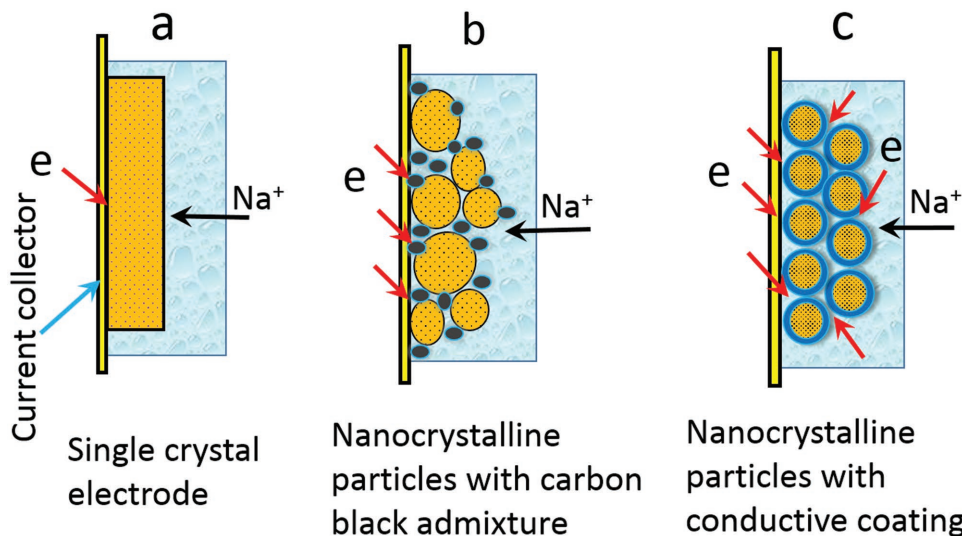


**Figure 2.** Schematic illustrations of various electrode morphologies: a) Large single crystal of a mixed conductor with insufficient storage kinetics. b) Nanocrystalline particles with carbon black admixture to optimize electronic transport allowing for electrolyte access. c) Conductive medium coated nanoparticles (using amorphous carbon or heteroatom doped carbon shell, graphene, carbon nanotube, etc.) for optimized storage. The electronically conductive coating is either conductive for ions as well or is porous (incomplete).

in affecting the transport to the particles via increasing  $\sigma_{ion}$  or  $\sigma_{eon}$ ; its influence on  $D_{eon}$  and on the  $\chi$  factor in Equation (2) is, if not negligible, then modest.<sup>[115]</sup> The most effective parameter is the particle size which enters quadratically. As a consequence, nano-structuring is a sensitive tool as also indicated by 2c. Please note that a value  $10^{-10} \text{ cm}^2 \text{ S}^{-1}$  leads to a storage time of about a minute for a particle size of  $1 \mu\text{m}$ , and to a value on the order of a second when the size is reduced to  $100 \text{ nm}$  (provided the other steps are fast enough).

## 2.2. NASICON Cathode Materials

### 2.2.1. Structure and Desodiation of $\text{Na}_3\text{V}_2(\text{PO}_4)_3$

The rhombohedral  $\text{Na}_3\text{V}_2(\text{PO}_4)_3$  (NVP) is characterized by space group  $R\bar{3}c$  and offers an open framework via NASICON structure. The basic constituents of the framework structure are  $[\text{VO}_6]$  octahedra and  $[\text{PO}_4]$  tetrahedra inter-linked via corner-sharing. Figure 3 displays the structure generated by VESTA with the lattice parameters  $a = b = 8.728 \text{ \AA}$  and  $c = 21.804 \text{ \AA}$ . This vanadium-based electrode shows two redox potentials at  $3.4 \text{ V}$  and  $1.6 \text{ V}$  characterized by  $\text{V}^{3+}/\text{V}^{4+}$  and  $\text{V}^{2+}/\text{V}^{3+}$  valence changes. As a consequence, this phosphate can be applied as both cathode and anode with relative theoretical capacities of  $117 \text{ mAh g}^{-1}$  and  $50 \text{ mAh g}^{-1}$ , respectively.<sup>[81]</sup>

The ion transport mechanism in NVP has been explored via first principles calculations.<sup>[82,116]</sup> According to this, the behavior is consistent with the well-known situation in the NASICON electrolytes.<sup>[89]</sup> There are two types of Na ions ( $\text{Na}_1$  located in a  $\text{V}_2(\text{PO}_4)_3$  environment along the c-axis,  $\text{Na}_2$  coordinated analogously but along b-axis) in the NVP crystal structure, as shown in Figure 3. Corresponding to the bond length data for  $\text{Na}-\text{O}$ ,<sup>[116]</sup> the sodium ions in the  $\text{Na}_2$  sites (2/3 occupancy) are more easily extracted than those on  $\text{Na}_1$  sites (1 occupancy) due

to the relatively weaker bonding. The Na ion-migration mechanism is detailed in Figure 4a–c.<sup>[82]</sup> The Na-extraction from  $\text{Na}_2$  sites result in pronounced structural reorganization until all the Na ions at  $\text{Na}_2$  sites are extracted. Unsurprisingly, the transition from  $\text{Na}_3\text{V}_2(\text{PO}_4)_3$  to  $\text{NaV}_2(\text{PO}_4)_3$  is not continuous, rather a two-phase reaction occurs under operation conditions.<sup>[82,117]</sup> Diffusion pathway 1, represented by the connected orange-green line of orange and green Na balls, proceeds in the (112) plane. Pathway 2, represented by the connected yellow-green line of yellow and green Na balls, takes place in the (121) plane as shown in Figure 4d.<sup>[117]</sup> The corresponding activation energy for the Na vacancy diffusion pathway 1 is given in 4d<sub>1</sub>. The black-green line connecting the Na at the  $\text{Na}_1$  sites and the Na vacancies ( $\text{vc}_1$  and  $\text{vc}_2$ ) represents pathway 3, referred to as inter-layer pathway (Figure 4e). According to the calculated activation energies of  $\text{vc}_1$  (513 meV) and  $\text{vc}_2$  (597 meV) in Figure 4e<sub>1</sub>, diffusion pathway 3 is preferred due to the low energy diffusion barrier.<sup>[117]</sup> Therefore, the diffusion of  $\text{Na}^+$  in NVP is mostly proceeding in the intra-layer with the hexagonal bottleneck as transition state in Figure 4e and e<sub>1</sub>.

Chen et al. report a direct experimental investigation of the Na extraction sites via aberration-corrected annular-bright-field scanning transmission electron microscopy (ABF-STEM).<sup>[118]</sup> The locations of sodium atoms in rhombohedral structures of  $\text{Na}_3\text{V}_2(\text{PO}_4)_3$  and  $\text{NaV}_2(\text{PO}_4)_3$  are shown in Figure 5a–b. While sodium atoms occupy both  $\text{Na}_1$  and  $\text{Na}_2$  sites in  $\text{Na}_3\text{V}_2(\text{PO}_4)_3$ , only  $\text{Na}_1$  sites are occupied in  $\text{NaV}_2(\text{PO}_4)_3$ , implying that it is the Na atoms at  $\text{Na}_2$  sites that are affected by the storage process. Figure 5c–d shows the corresponding line profiles for  $\text{Na}_3\text{V}_2(\text{PO}_4)_3$  and  $\text{NaV}_2(\text{PO}_4)_3$ . The distance parameters in the line profiles of  $\text{Na}_3\text{V}_2(\text{PO}_4)_3$  are different, corresponding to  $0.45 \text{ nm}$  and  $0.61 \text{ nm}$  for  $d_1$  and  $d_2$ , respectively. This is ascribed to the occupation at  $\text{Na}_2$  sites. However, the distance parameter in the line profile of  $\text{NaV}_2(\text{PO}_4)_3$  is the same ( $d_3 = d_4 = 0.41 \text{ nm}$ ), indicating location at  $\text{Na}_1$  sites. The

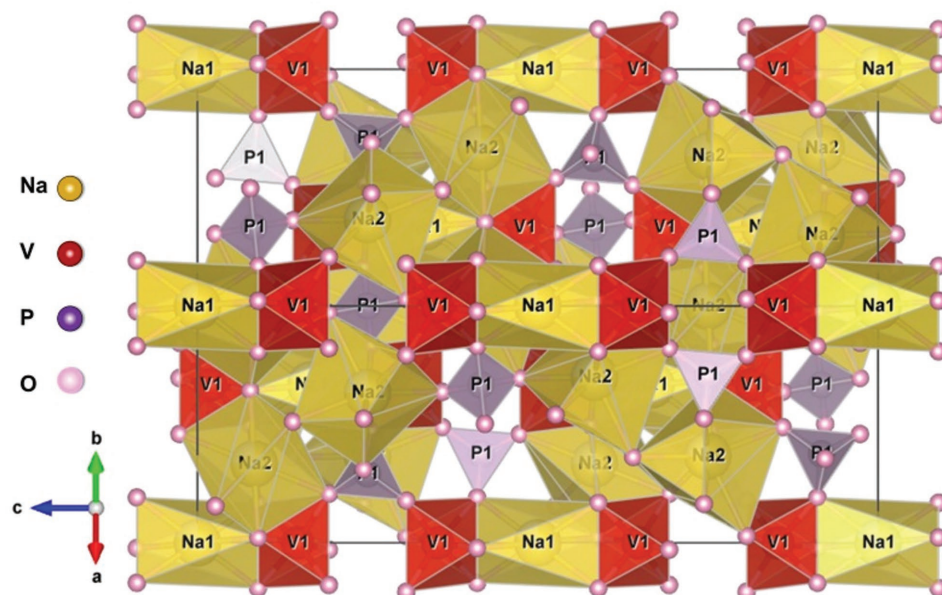


**Figure 3.** Crystal structure of  $\text{Na}_3\text{V}_2(\text{PO}_4)_3$  (110-face).

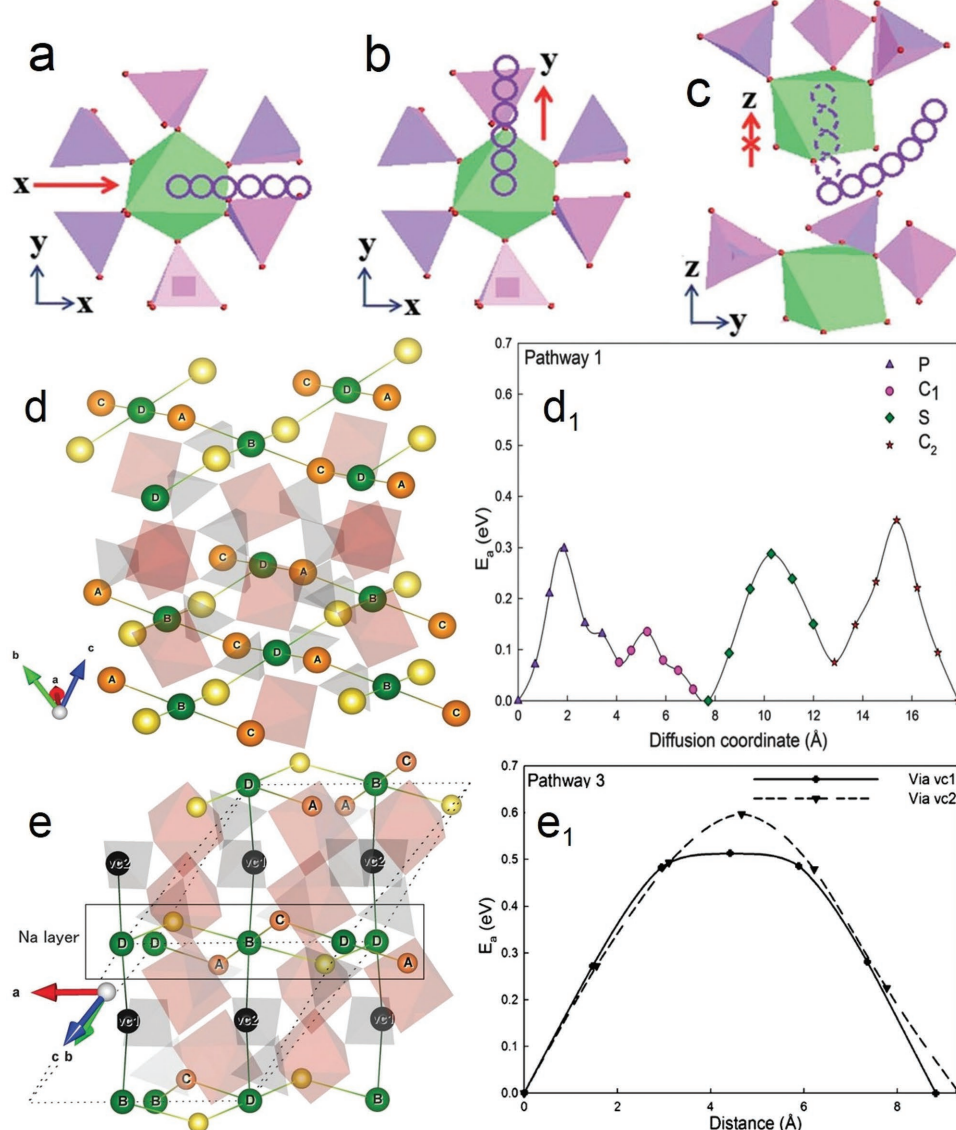


**Figure 4.** Possible Na ion migration paths in NVP along (a) x, (b) y and (c) curved z directions. d) Schematic depiction of pathways 1 and 2 of  $\text{Na}^+$  in the NVP crystals. The orange-green lines that connect orange and green Na balls represent pathway 1, and the yellow-green lines that connect yellow and green Na balls represent pathway 2. e) The black-green lines that connect Na at the  $\text{Na}_1$  site and the Na vacancies ( $\text{vc}_1$  and  $\text{vc}_2$ ) represent pathway 3. e<sub>1</sub>) Activation energies of  $\text{vc}_1$  and  $\text{vc}_2$  along pathway 3.<sup>[82,117]</sup> Copyright 2014, 2015 Royal Society of Chemistry.

Na ion extraction scheme for  $\text{Na}_3\text{V}_2(\text{PO}_4)_3$  are given by Ji et al. is depicted in Figure 5e.<sup>[119]</sup> The (de)sodiation process is accompanied by and characterized by a theoretical capacity of 117.6 mAh g<sup>-1</sup> and a moderate volume change of 8.26%.<sup>[120]</sup>

The good thermal stability of  $\text{Na}_3\text{V}_2(\text{PO}_4)_3$  is of great significance for long term cycling and large-scale applications due to the occurring temperature variations. Only slight weight losses for  $\text{Na}_3\text{V}_2(\text{PO}_4)_3$  (1.6%) have been found by Choi et al. using thermogravimetric analysis and differential scanning calorimetry (DSC). When the temperature was increased up to 450 °C, no endothermic/exothermic peak was discovered in DSC curves. The high thermal stability also offers the possibility to increase operation temperature as to improve reaction resistances.

## 2.2.2. Preparation and Electrochemical Performance of $\text{Na}_3\text{V}_2(\text{PO}_4)_3$

As discussed above, the  $\text{Na}_3\text{V}_2(\text{PO}_4)_3$  particles require a small particle size and contacting by an electronically conductive medium to improve the overall transport. As to the conductive medium, carbon materials (such as thin carbon layers, hollow carbon nanospheres, carbon nanotubes, graphene, mesoporous ordered carbon frameworks and interconnected carbon frameworks etc.) have been shown to be favorable not only in improving the grain conductivity but also in preventing particle agglomeration and electrode polarization during long-term cycles at high current densities.<sup>[81,108,121–127]</sup> Doped carbon materials (by nitrogen, boron, etc.) seems particularly

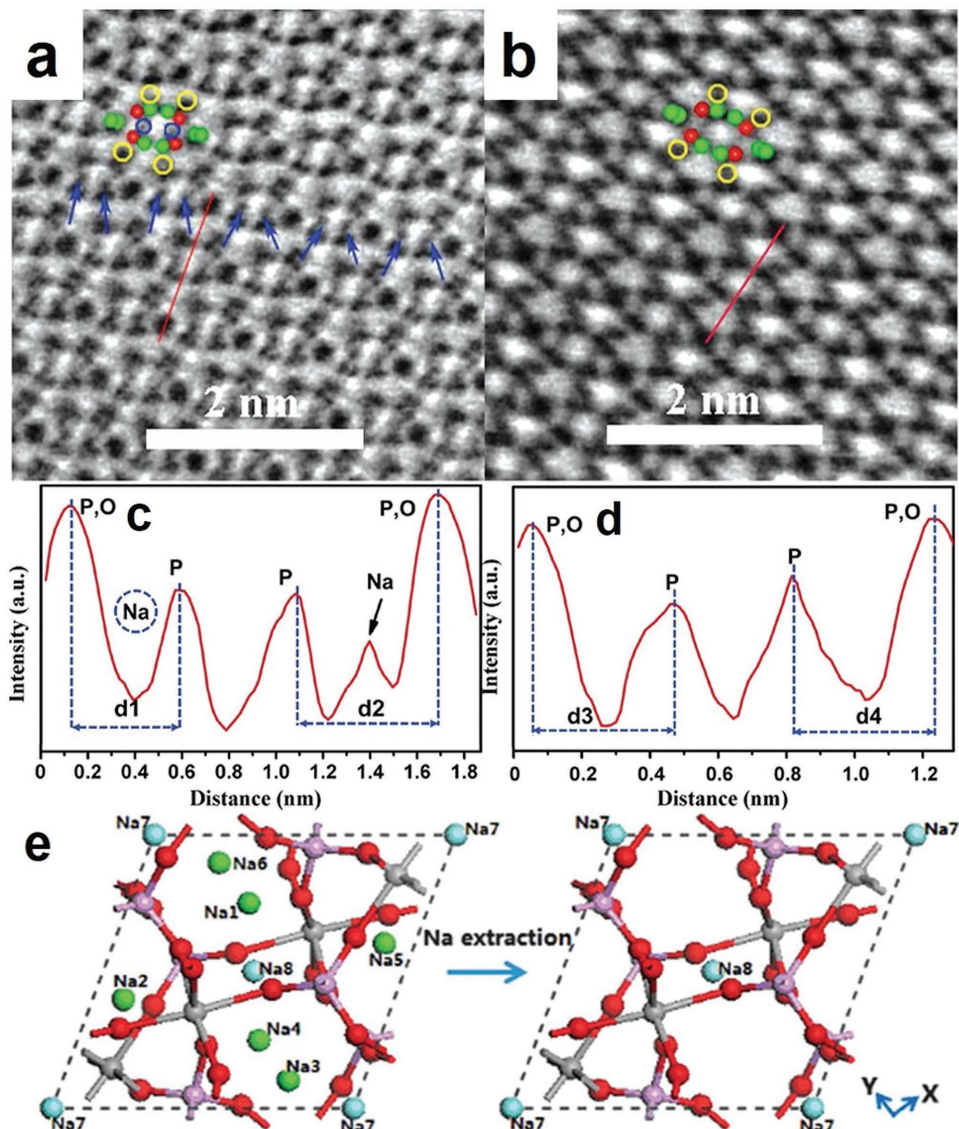


**Figure 5.** STEM ABF images of (a)  $\text{Na}_3\text{V}_2(\text{PO}_4)_3$  and (b)  $\text{Na}_3\text{V}_2(\text{PO}_4)_3$  in the  $[111]$  projection (blue and yellow circles represent Na atoms at Na1 and Na2 sites, respectively, and the blue arrow stands for the Na atoms at Na2 site). Line profiles along in the ABF images of (c)  $\text{Na}_3\text{V}_2(\text{PO}_4)_3$  and (d)  $\text{Na}_3\text{V}_2(\text{PO}_4)_3$ , where the images contrast of the dark dot are inverted and displayed as peaks.<sup>[118]</sup> e) Na extraction scheme. Reproduced with permission.<sup>[119]</sup> Copyright 2014, Royal Society of Chemistry.

favorable.<sup>[110,128,129]</sup> The various approaches to enhance the overall electrical conductivity of NVP are shown in Figure 6a–f.

**2.2.2.1. Size Reduction and Coating of  $\text{Na}_3\text{V}_2(\text{PO}_4)_3$ :** Size and homogeneity of the carbon coating are not easy to control in the preparation process. The typical preparation of NVP involves a high temperature annealing process, during which crystal growth occurs. Organic polymers and surfactants are frequently used to control the NVP size; they reduce surface tension of solvents and can simultaneously serve as carbon sources.<sup>[130]</sup> Chen et al. compared the electrochemical differences of bulk NVP particles, carbon coated NVP particles (NVP@C) and carbon coated NVP nanoparticles (Nano NVP@C).<sup>[131]</sup> Owing to the low electrical conductivity of both bulk NVP and large NVP@C composites,

sodiation/desodiation processes only occurred in the outer shells of the big particles, leaving a large inactive volume in the cores of the particles as illustrated in Figure 7a. Figure 7b displays morphologies of NVP nanoparticles studied by Mai and coworkers.<sup>[122]</sup> Thin carbon layers homogeneously coating NVP nanoparticles are shown in Figure 7b. Figure 7c–d display 3D carbon coated NVP nanofiber (diameters of 20–80 nm) networks (NVP-F) that are well maintained after annealing at 700 °C as demonstrated by TEM and HRTEM images. A thin well-defined carbon layer with a thickness of  $\approx 3$  nm formed on the surface of NVP nanofiber networks.<sup>[132]</sup> The rate capacities of such NVP-F nanofiber networks were found to be superior to that of the NVP microflowers and of dense NVP bulk materials. Jian et al. reported carbon coated NVP nanoparticles as sodium electrodes with a thickness of 5 nm for carbon layer,

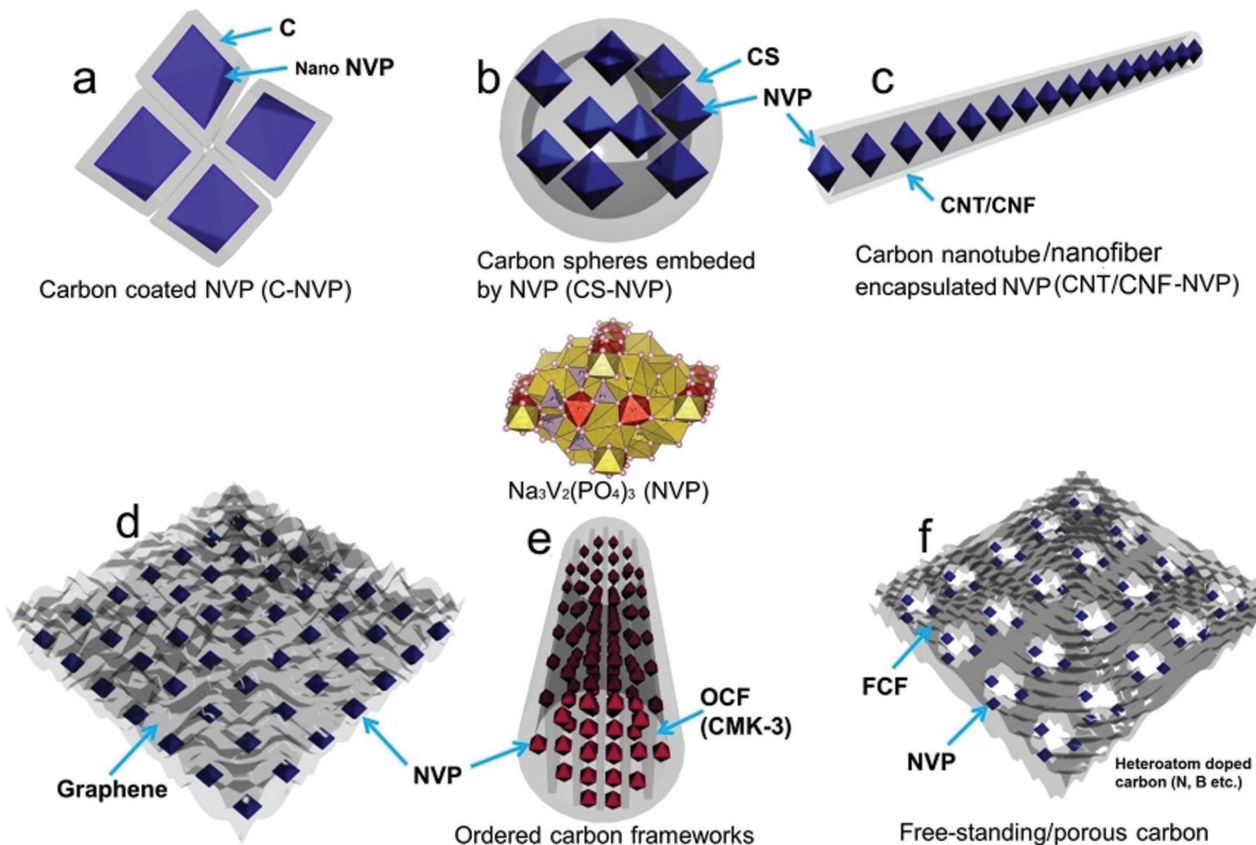


**Figure 6.** The scheme of modifying  $\text{Na}_3\text{V}_2(\text{PO}_4)_3$  particles via different approaches to enhance the conductivity of composites, including minimizing particles size (a), porous carbon spheres embedded NVP (b), carbon nanotube/nanofiber encapsulated NVP nanoparticles (c), graphene film supported NVP nanoparticles (d), ordered carbon framework (CMK-3) encapsulated NVP nanoparticles (e), free-standing/porous carbon supported NVP nanoparticles or heteroatoms (N, B etc.) doped carbon frameworks carried NVP nanoparticles (f). Note that electrolyte access to the electroactive mass must be guaranteed in all these cases.

showing impressive electrochemical performances of anode materials.<sup>[127]</sup>

Following a general strategy by Yu and co-workers to optimize transport and minimize side reactions, NVP nanoparticles are homogeneously embedded in 1D nanofibers via the electrospinning technique, as shown in Figure 7e.<sup>[125]</sup> Citric acid (also serving as size-controlling agent) and polyethylene oxide (as carbon source) serve as carbon source. The tiny NVP particles with an average diameter of 10 nm, homogeneously dispersed in the typical 1D nanofiber, illustrated by the TEM image in Figure 7f. The 1D NVP-F@C nanofiber material exhibits very good rate capacities even in the current window of 2 C to 20 C. A similar behavior is reported by Hosono et al. using 1D carbon sheaths to confine the small NVP particles via electrospinning.<sup>[133]</sup> The NVP nanoparticles are in situ formed in the carbon sheath and uniformly dispersed in thin mesoporous carbon layers. They deliver a high capacity of 94 mAh·g<sup>-1</sup> and a good cycling performance within 50 cycles. To minimize the particle size, Kim et al. applied a polyol-mediated method for the synthesis of carbon coated NVP nanoparticles.<sup>[134]</sup> Such carbon layers prevent particles from growing and aggregating at high temperatures. Similar attempt has been undertaken by Chen et al.<sup>[120]</sup> In this work the surface of NVP

crystal was coated by a thin carbon shell of a thickness of 3 nm, resulting in a good cycling performance. Obviously, size variation and coating are not only promising but also helpful tools in improving the storage kinetics.

**2.2.2.2. Combining  $\text{Na}_3\text{V}_2(\text{PO}_4)_3$  with Various Carbon Materials:** Various carbon materials have been reported as conductive substrates to improve the properties of electrodes. They can provide attractive features such as high surface area, high electrical conductivity, good chemical stability and low cost.<sup>[135,136]</sup> Here, we deal with five typical carbon materials that have been used to enhance the electrochemical features of NVP, (Figure 6a–f): amorphous carbon, CNT, graphene, mesoporous ordered carbon (CMK-3), and interconnected carbon frameworks.

- i) Amorphous carbon can be obtained from many organic polymers, polysaccharides or surfactants by annealing them in inert atmosphere. Amorphous carbon, derived from vanadyl acetylacetone, was shown to completely coat NVP nanoparticles,<sup>[123]</sup> and to form the double-carbon-embedding structure shown in Figure 8a. The NVP nanoparticles coated by thin carbon layers exhibit exceptional electrochemical performance. Figure 8b displays the

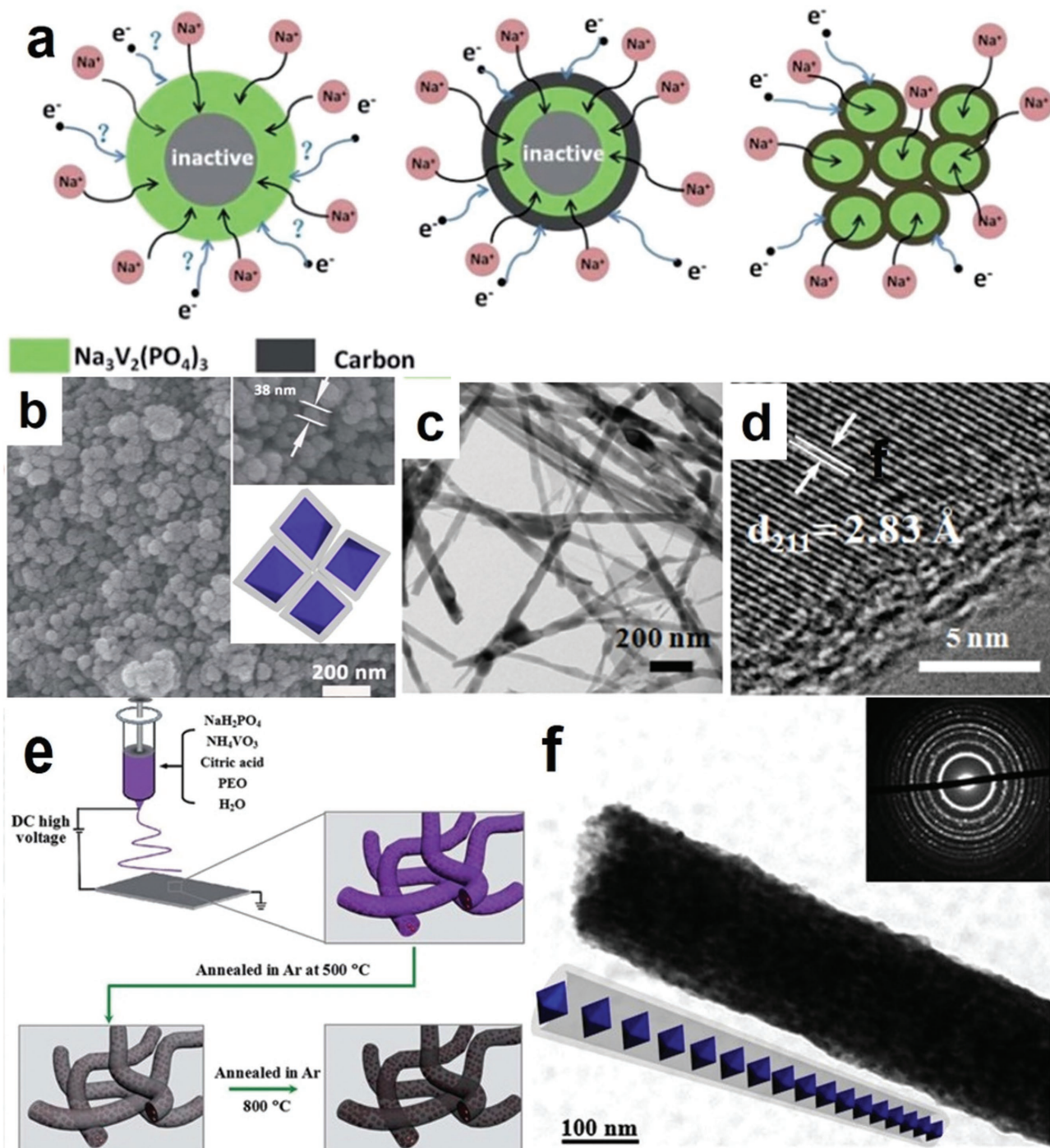


**Figure 7.** a) Significance of providing electronic pathways in the nanoparticle ensemble (gray zones represent inactive sections due to the limited electron transfer paths). b) SEM and HRTEM images of Nano-NVP@C composites with core-shell structure. Reproduced with permission.<sup>[131]</sup> Copyright 2014, Royal Society of Chemistry. c, d) TEM and HRTEM images of  $\text{Na}_3\text{V}_2(\text{PO}_4)_3$  nanofibers (NVP-F) networks. Reproduced with permission.<sup>[122]</sup> Copyright 2016, Elsevier. e) Preparation scheme for NVP nanofibers. f) TEM and HRTEM images of NVP nanofibers with SAED pattern as insert. Reproduced with permission.<sup>[125]</sup> Copyright 2014, Royal Society of Chemistry.

influences of amorphous carbon, carbon nanotube and graphite on the capacity of NVP nanoparticles according to Mai et al.<sup>[137]</sup> In all three cases, NVP nanoparticles are well distributed in the carbon materials. The corresponding electrochemical performance is highest for the

NVP/amorphous carbon composite, which is attributed to its uniform coating.

- ii) Carbon nanotubes (CNTs) consist of a carbon allotrope with excellent electrical conductivity, mechanical property and good thermal stability, and thus a good candidate as

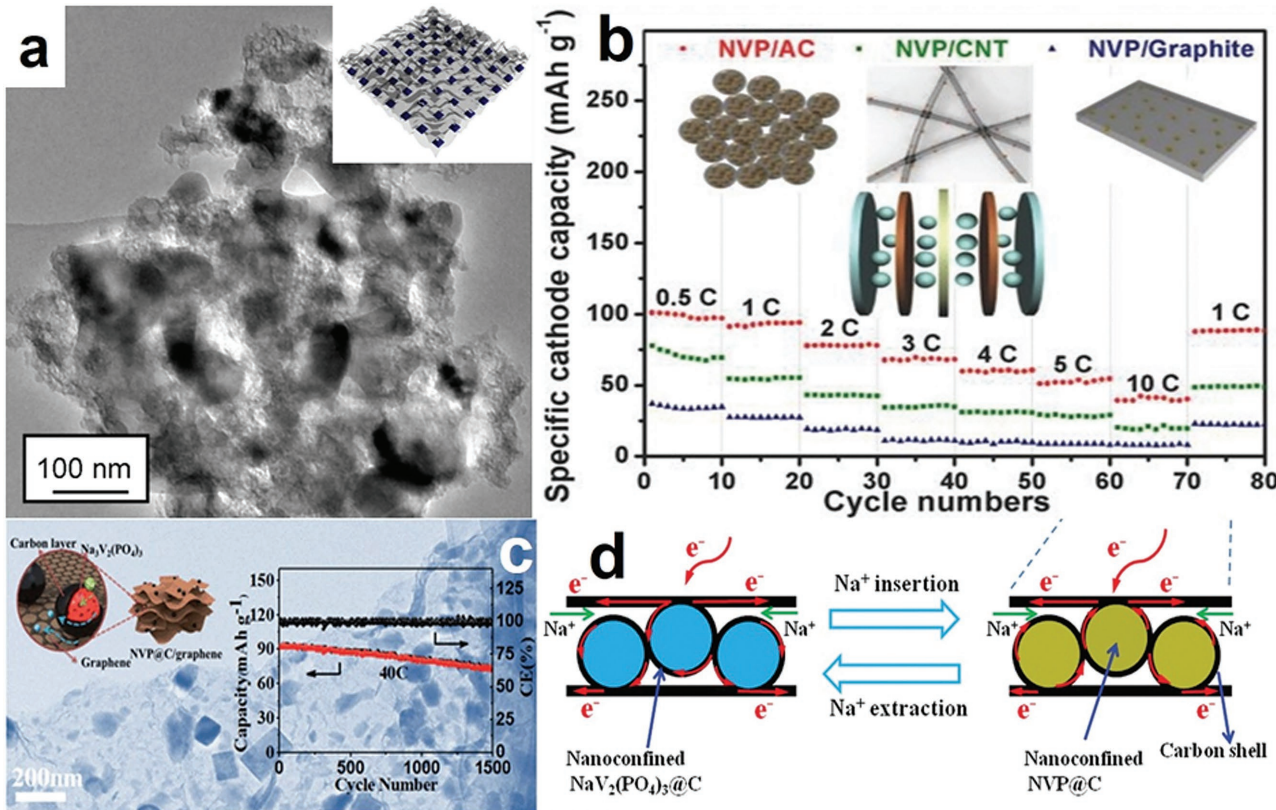


**Figure 8.** a) TEM images of double carbon embedding NVP (C@NVP@pC) composites. Reproduced with permission.<sup>[123]</sup> Copyright 2014, American Chemical Society. b) The scheme and rate capacities of amorphous carbon, CNT and graphite coated NVP composites. Reproduced with permission.<sup>[137]</sup> Copyright 2014, Wiley-VCH. c) The TEM image and cycling performance of carbon coated NVP/graphene composites. Reproduced with permission.<sup>[108]</sup> Copyright 2016 Royal Society of Chemistry. d) The scheme de-/sodiation of NVP/CMK-3 composites.<sup>[121]</sup>

- current-collecting phase. Commercial multi-walled CNTs were mixed with NVP precursor, and then ball-milled to prepare homogeneous composites.<sup>[124]</sup> Compared to the carbon coated NVP, the MCNT/NVP@C composites (MCNT, 2 wt%) are well connected by MCNTs, showing a higher capacity of 146.5 mAh g<sup>-1</sup>, and maintaining a high capacity retention ratio of 94.3% even after 50 cycles. This favorable behavior is mainly due to the addition of MCNT serving as charge transfer mediator.
- iii) Graphene is, in the ideal case, one kind of 2D one-atom-thick and  $sp^2$ -bonded carbon sheet, which has applications in many research fields because of its good thermal stability, superior electronic conductivity, and high specific surface area.<sup>[138–144]</sup> Zhu et al. developed a 3D meso- and macro-porous carbon coated NVP-graphene (NVP@C@rGO) architecture via freezing-dry technique, in which the carbon shell on NVP was derived from carbonization of poly(vinyl pyrrolidone).<sup>[145]</sup> The NVP@C@rGO composites exhibited exceptional electrochemical performances, including high capacities (115, 112, 103, 91 and 86 mAh g<sup>-1</sup> at the current rates of 1, 20, 50, 80 and 100 C, respectively) and stable cycling performance after 10k cycles at 100 C (ultra-slow capacity fading rate, 0.0045% per cycle). The very good electrochemical performance is intimately connected with the nanocrystallinity of the NVP particles, and the combination of highly conductive carbon network consisting of

inter-connected graphene layers and thin carbon shells. A similar strategy was applied by Wang et al., using citric acid as chelating agent and carbon source to form a thin carbon layer on the surface of NVP.<sup>[108]</sup> The 3D graphene network prepared by freeze-drying is illustrated in Figure 8c. The carbon coated NVP nanoparticles are homogeneously distributed between graphene sheets, remaining well-dispersed during high temperature annealing. The NVP@C-G composites delivered a high capacity of 86.5 mAh g<sup>-1</sup> at 40 C with a capacity retention ratio of 82% after 1500 cycles.

- iv) Ordered carbon framework: highly ordered mesoporous carbon materials have been developed in many areas due to the high surface area, uniform porosity, well-interconnected framework and excellent electrical conductivity.<sup>[146–149]</sup> These advantages make an ordered carbon framework an ideal matrix to encapsulate NVP nanoparticles. Yu and co-workers synthesized carbon-coated NVP nanoparticles, which are embedded in CMK-3 chambers (NVP@C@CMK-3).<sup>[121]</sup> In this NVP@C@CMK-3 material, CMK-3 and thin carbon shells on NVP provided fast electron/Na<sup>+</sup> transfer channels to individual NVP nanoparticles during charge/discharge as shown in Figure 8d.
- v) Interconnected carbon frameworks result in free-standing and binder-free features, and can be prepared via various methods such as electrostatic spray deposition (ESD), spray-drying, and filtration-freezing-drying techniques. For

example, 3D tri-continuous free-standing NVP/rGO/CNT networks could be prepared by the ESD technique without using binders and current collectors.<sup>[81]</sup> The high porosity and interconnectivity make the homogeneously distributed NVP nanoparticles show excellent electrochemical performance. The NVP/rGO/CNT electrode delivered excellent rate capabilities (high capacities of 109 mAh g<sup>-1</sup> and 82 mAh g<sup>-1</sup> at 30 C and 100 C, respectively) and exceptional cycling performances. Ultra-fast charge/ionic transport networks are formed when all the pores are filled with electrolyte. Although there are large differences on preparation techniques for different NVP/carbon materials, all these NVP/carbon composites show improved electrochemical performances compared to bulk NVP.

Compared to the compositionally pure carbon materials, N- or B-doped carbon exhibits much higher electrical conductivity.<sup>[150–155]</sup> For the nitrogen doped carbon materials, there are generally three types of binding configurations, including pyridinic N, pyrrolic N and quaternary N (or graphitic N). i) Pyridinic N is connected to two adjacent C atoms at the edges or vacancies, contributing one p electron to  $\pi$  system and showing a sp<sup>2</sup> hybridized structure. ii) Pyrrolic N contributes two p electrons to the  $\pi$  system with a sp<sup>3</sup> hybridized structure, now forming five-membered rings. iii) Quaternary N is formed by substituting one C in a hexagonal ring acting as n-type dopant and leading to sp<sup>2</sup> hybridization.<sup>[155–159]</sup> Most importantly, all the three types of N doping will influence the conductivity of carbon coating layers on the targeted materials; both pyridinic N and pyrrolic N create atomic defects and active sites for sodium storage.<sup>[155]</sup> Interestingly these three states correspond to atomically and electronically compensated heterovalent doping and to homovalent doping (elastic effects).<sup>[160]</sup> Wang et al. prepared N-doped carbon coated NVP (NVP-C-N) nanoparticles and discussed different electrochemical performances on the basis of different nitrogen/carbon ratios.<sup>[128]</sup> The HRTEM image in Figure 9a exhibits the crystal structure of such a N-doped NVP-C-N142 sample. N-doped carbon shells with thicknesses of  $\approx$ 5 nm are observed. The N-doped NVP-C-N142 sample delivered the highest specific capacity of 101.9 mAh g<sup>-1</sup> at 0.2 C and showed excellent rate capacities (from 0.2 C to 5 C), as well as stable cycling performance (maintained 92.6% of initial capacity after 100 cycles at 5 C). The corresponding scheme is illustrated by Figure 9b, according to which sodium preferentially travels through vacancies caused by N-doping on carbon shells. Note that in undoped carbon, sodium shows poor ion

electrons to the  $\pi$  system with a sp<sup>3</sup> hybridized structure, now forming five-membered rings. iii) Quaternary N is formed by substituting one C in a hexagonal ring acting as n-type dopant and leading to sp<sup>2</sup> hybridization.<sup>[155–159]</sup> Most importantly, all the three types of N doping will influence the conductivity of carbon coating layers on the targeted materials; both pyridinic N and pyrrolic N create atomic defects and active sites for sodium storage.<sup>[155]</sup> Interestingly these three states correspond to atomically and electronically compensated heterovalent doping and to homovalent doping (elastic effects).<sup>[160]</sup> Wang et al. prepared N-doped carbon coated NVP (NVP-C-N) nanoparticles and discussed different electrochemical performances on the basis of different nitrogen/carbon ratios.<sup>[128]</sup> The HRTEM image in Figure 9a exhibits the crystal structure of such a N-doped NVP-C-N142 sample. N-doped carbon shells with thicknesses of  $\approx$ 5 nm are observed. The N-doped NVP-C-N142 sample delivered the highest specific capacity of 101.9 mAh g<sup>-1</sup> at 0.2 C and showed excellent rate capacities (from 0.2 C to 5 C), as well as stable cycling performance (maintained 92.6% of initial capacity after 100 cycles at 5 C). The corresponding scheme is illustrated by Figure 9b, according to which sodium preferentially travels through vacancies caused by N-doping on carbon shells. Note that in undoped carbon, sodium shows poor ion

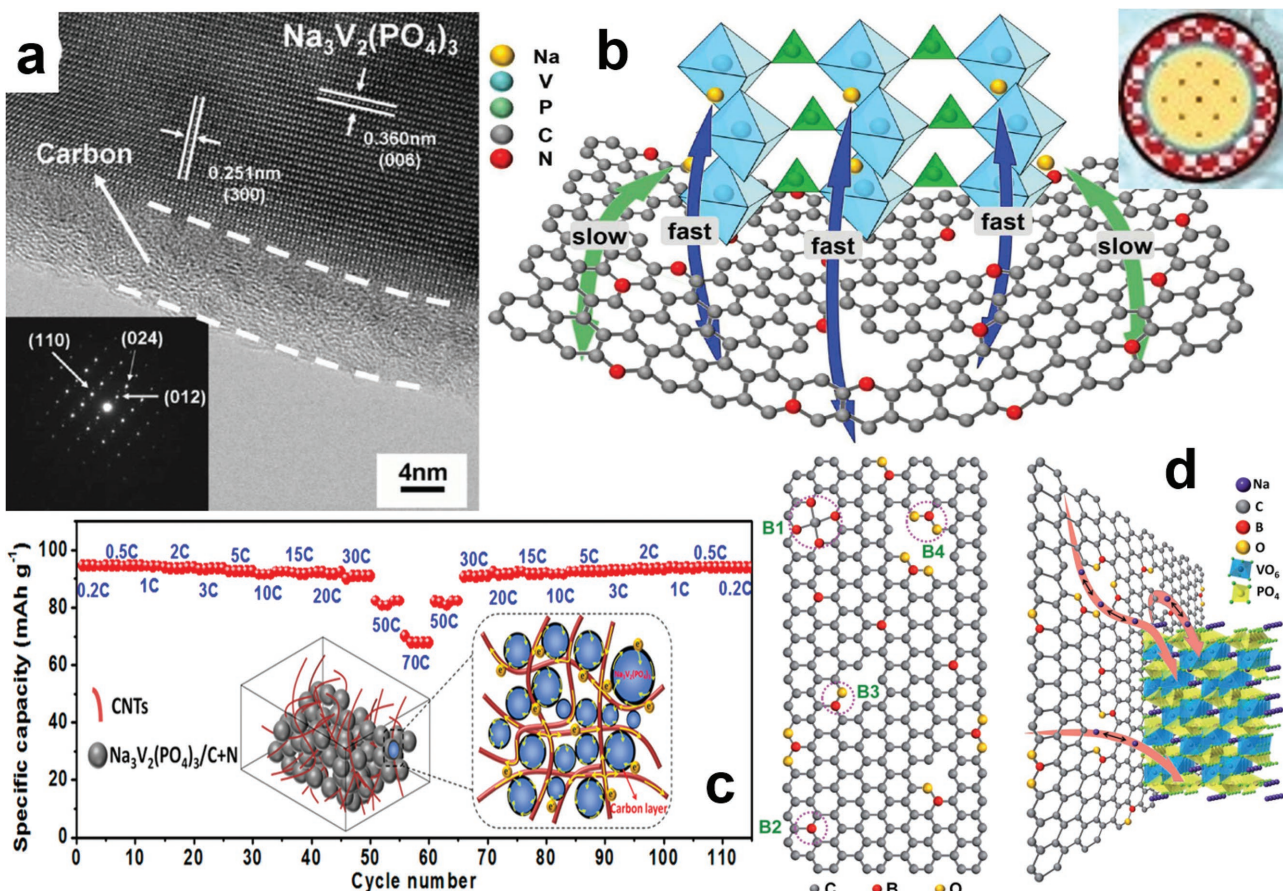


**Figure 9.** The HRTEM image and SAED pattern of NVP-C-N142 (a). Scheme of Na diffusion and electron transfer path (b). Reproduced with permission.<sup>[128]</sup> Copyright 2014, WILEY-VCH. Rate capability of NVP@C-N@CNT composite (c). Reproduced with permission.<sup>[129]</sup> Copyright 2016, American Chemical Society. d) Schematic illustration of structure and storage mechanism of NVP-C-B0.38%. Reproduced with permission.<sup>[110]</sup> Copyright 2015 Royal Society of Chemistry.

diffusivity. Indeed, previous work indicated that the N-doped carbon shell not only increases the effective electronic conductivity, but also enhances ionic diffusion during charging and discharging.<sup>[161–163]</sup> A similar strategy is applied to the synthesis of N-doped NVP@CNT (NVP@C-N@CNT) composites by Wang et al.<sup>[129]</sup> From the schematic image in Figure 9c, one can deduce that N-doped CNTs are arranged as self-connected network wrapping the NVP nanoparticles. These NVP@C-N@CNT composites exhibited exceptional rate capabilities from 0.2 C to 70 C, which are also ascribed to the extrinsic defects generated by the N-doping.

Notwithstanding the fact that the N-doped carbon coated NVP materials have shown exceptional electrochemical performance, the N-doped carbon materials are relatively sensitive to moisture and oxygen, which unfavorably affects their conductivity. Boron-doped carbon materials prepared by using boron trichloride ( $\text{BCl}_3$ ), borane-tetrahydrofuran adduct ( $\text{BH}_3\text{-THF}$ ) or boron oxide ( $\text{B}_2\text{O}_3$ ) as boron agent have demonstrated high conductivity regardless of environment influence.<sup>[164–169]</sup> For example, Wang et al. used sodium tetraphenylborate ( $\text{NaBC}_{24}\text{H}_{20}$ ) as boron source to prepare the boron-doped carbon coated NVP (NVP-C-B) composites via a facile sol-gel approach.<sup>[110]</sup> The typical HRTEM image and SAED pattern of the NVP-C-B0.38% samples show high crystallization degree of NVP and a uniformly coated carbon shell with an average thickness of  $\approx 5$  nm. The NVP-C-B0.38% composite exhibited better rate capabilities than other NVP-C-B and NVP-C composites, and lower

over-voltages (from 0.09 V, 0.15 and 0.36V, respectively). A high amount of doped B could substantially increase the diffusion rate of sodium ions in the carbon layer. A structure of B-doped carbon layer and  $\text{Na}^+$  diffusion are sketched in Figure 9d. The NVP-C-B0.38% composite was reported to show the lowest electrochemical impedance owing to quick charge transfer and fast  $\text{Na}^+$  ion diffusion. Evidently, doping of carbon is another effective tool to improve transport kinetics.

### 2.2.3. Properties and Desodiation of $\text{Na}_3\text{V}_2(\text{PO}_4)_2\text{F}_3$

Replacing one  $(\text{PO}_4)_3^-$  anion from NVP by 3  $\text{F}^-$ ,  $\text{Na}_3\text{V}_2(\text{PO}_4)_2\text{F}_3$  (NVPF) is formed crystallizing in the rhombohedral NASICON structure, but exhibiting the space group  $P\bar{4}_2/mnm$ . NVPF is built by  $[\text{V}_2\text{O}_8\text{F}_3]$  bi-octahedra and  $[\text{PO}_4]$  tetrahedra, inter-linked via corner-sharing. The corresponding atomic structure is presented in Figure 10a (projected on the  $bc$  plane) and 10a<sub>1</sub> (projected on the  $ab$  plane) with lattice parameters of  $a = b = 9.042 \text{ \AA}$  and  $c = 10.749 \text{ \AA}$ , providing convenient diffusion channels for Na ions.<sup>[170]</sup> In this open framework structure fully occupied Na sites are named as  $\text{Na}_1$  sites and half-occupied Na sites are denoted as  $\text{Na}_2$ ; the occupancy ratio between them is 2:1. As three fluorine atoms replace one phosphate group, additional interstitial spaces for fast diffusion of sodium ions is formed.<sup>[171]</sup> Owing to the extreme electronegativity of F, the compound shows higher redox potentials for de-/sodiation,

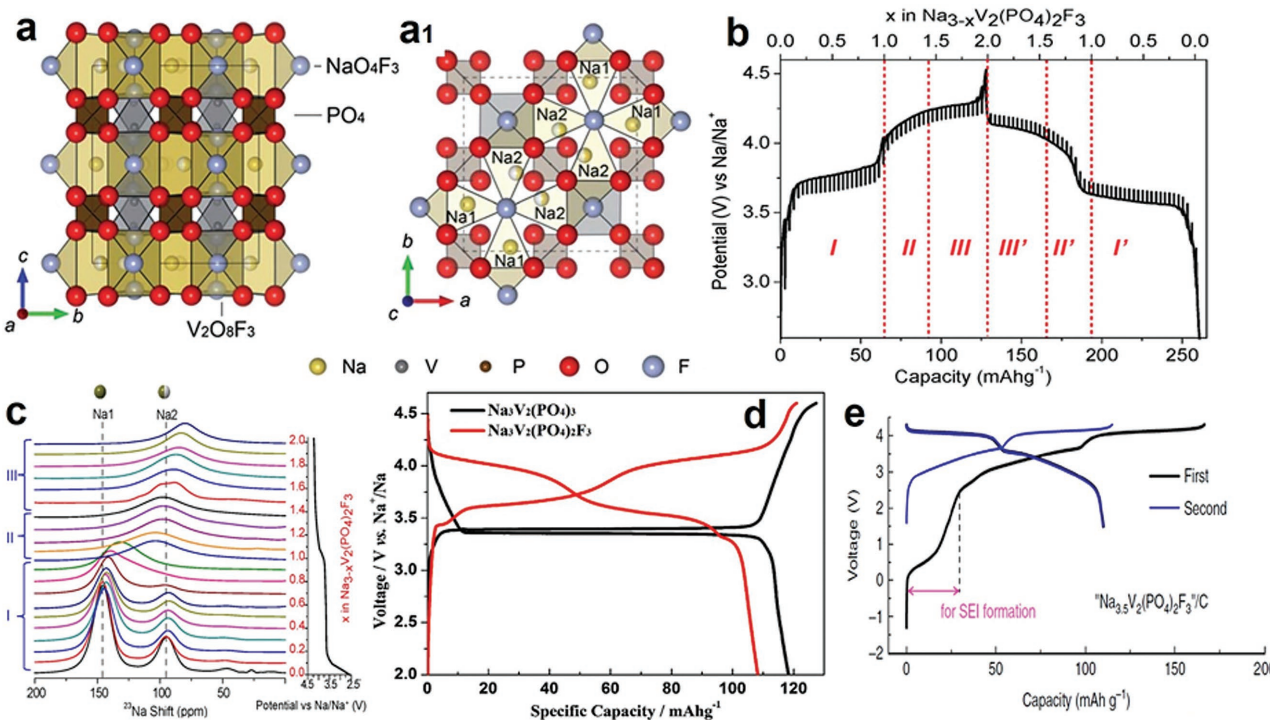
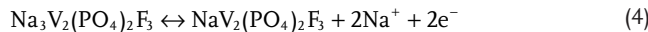


**Figure 10.** Illustration of  $\text{Na}_3\text{V}_2(\text{PO}_4)_2\text{F}_3$  projected on  $bc$  plane (a) and on  $ab$  plane (a1). Reproduced with permission.<sup>[170]</sup> Copyright 2012, Royal Society of Chemistry. Galvanostatic intermittent titration technique plot (b). c) Ex situ  $^{23}\text{Na}$  NMR spectra of  $\text{Na}_3\text{V}_2(\text{PO}_4)_2\text{F}_3$  at different charge state. Reproduced with permission.<sup>[173]</sup> Copyright 2014, American Chemical Society. d) Galvanostatic charge/discharge profiles of  $\text{Na}_3\text{V}_2(\text{PO}_4)_3$  and  $\text{Na}_3\text{V}_2(\text{PO}_4)_2\text{F}_3$  at 0.1 C. Reproduced with permission.<sup>[176]</sup> Copyright 2014, Elsevier. e) The voltage-profile of NVPF and  $\text{Na}_3.5\text{V}_2(\text{PO}_4)_2\text{F}_3/\text{C}$ , respectively. Reproduced with permission.<sup>[179]</sup> Copyright 2016, Nature Publishing Group.

namely 3.9 V and 4.28 V, and good thermal stability.<sup>[172]</sup> The full desodiation follows the equation:<sup>[173,174]</sup>



The charge/discharge process was studied by galvanostatic intermittent titration technique (GITT) and <sup>23</sup>Na NMR (cf. Figure 10b and c).<sup>[173]</sup> According to the authors, the results show that sodium extraction of NVPF, in fact, undergoes three reaction stages (with a theoretical capacity of 128 mAh g<sup>-1</sup>), including extraction of Na ions non-selectively from the two distinct Na sites at stage I (from 3.6 to 3.7 V) and stage II and III (from 3.7 to 4.05, and 4.5V, respectively), at least at the beginning of the charging process. The ex situ <sup>23</sup>Na NMR patterns (Figure 10c) exhibit no apparent peak shifts but a significant decrease in peak intensity and linewidth broadening (after x = 0.3) at stage I, furthermore obvious peak shifts, decreasing in intensities, at stage II and III with new peaks emerging at lower resonances. There is no apparent preference for Na removal (or insert) at Na<sub>1</sub> and Na<sub>2</sub> sites during the earlier stage of charge (or later stage of discharge), which contradicts earlier literature reports.<sup>[170,175]</sup> Compared to the charge/discharge profile of Na<sub>3</sub>V<sub>2</sub>(PO<sub>4</sub>)<sub>3</sub>, the Na<sub>3</sub>V<sub>2</sub>(PO<sub>4</sub>)<sub>2</sub>F<sub>3</sub> compound shows higher charge voltage plateaus at 3.66, and 4.1 V vs Na/Na<sup>+</sup> during charge. The voltage-profile difference between NVP and NVPF is shown in Figure 10d.<sup>[176]</sup> Additionally, NVPF exhibits extremely low volumetric changes (1.79%), even lower than most lithium cathode materials and exceptional thermal stability with only 5% weight loss up to 550 °C, implying fast diffusion of Na ions and minimal structural distortion, all promising aspects for safe SIBs.<sup>[170]</sup>

As in most batteries the stability relies on solid electrolyte interphases (SEI), the SEI layer on NVPF has been studied by various researchers.<sup>[177-179]</sup> The formation of SEI consumes sodium ions during initial charge (Figure 10e). According to ref. [179] an apparent charge hysteresis appears in the first cycles but is absent in the following cycles. This indicates irreversible formation of stationary SEI on the surface of the carbon electrode. The substantial cycling performances of a sodium-treated Na<sub>3.5</sub>V<sub>2</sub>(PO<sub>4</sub>)<sub>2</sub>F<sub>3</sub>/C full battery is better than that of normal NVPF full batteries in terms of both capacity and cycling performance.<sup>[179]</sup> Another approach to enhance the cyclability uses a pre-sodiated anode to avoid consumption of Na ions from the cathode. In ref. [105,180-182], both cathode and anode electrodes are pre-treated to form stable SEI layers.

Similar to NVP, NVPF also shows low electronic conductivity. Thus the performance of NVPF compounds can be greatly improved by coating with carbon (using carbon black or citric acid as precursor and size-control agent) to enhance the electrical conductivity. Song et al. prepared amorphous carbon coated NVPF (NVPF@C) nanoparticles via the carbon-thermal reduction method.<sup>[183]</sup> These NVPF@C nanoparticles delivered a high discharge capacity of 114.6 and 111.6 mAh g<sup>-1</sup> at 0.045 C and 0.091 C, and maintained a capacity retention ratio of 97.6% after 50 cycles with a high Coulombic efficiency of 98%. Another example is reported by Du et al. using citric acid as carbon source.<sup>[184]</sup> NVPF@MC composites with a thin carbon shell (7 nm) delivered a high capacity of ≈130 mAh g<sup>-1</sup> over 50 cycles, and exhibited good rate capacities up to 30 C.<sup>[172]</sup>

#### 2.2.4. Other NASICON Cathode Materials

Besides NVP and NVPF, there are many other interesting materials following the general NASICON formula Na<sub>x</sub>MM'(XO<sub>4</sub>)<sub>3</sub> (M = V, Ti, Fe, Tr or Nb; X = P, or S, x = 0-4), such as

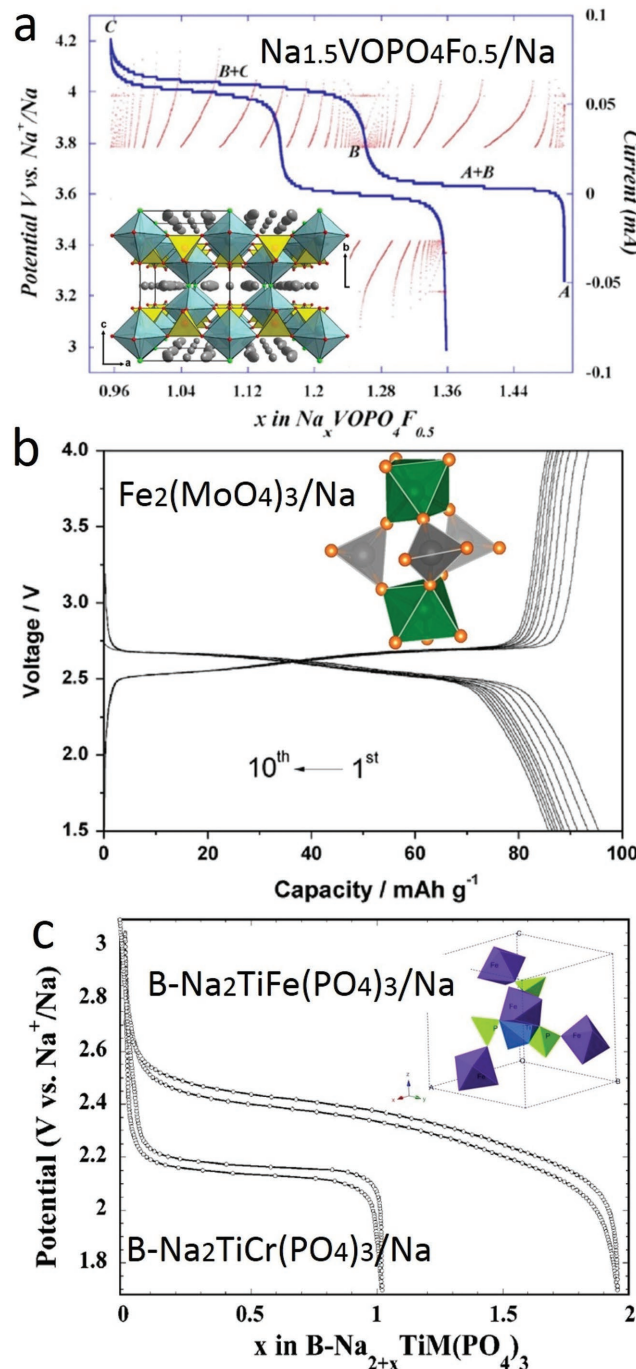


**Figure 11.** a) Voltage-profile of  $\text{Na}_{1.5}\text{VOPO}_4\text{F}_{0.5}$  and structure model. Reproduced with permission.<sup>[186]</sup> Copyright 2006, Elsevier. b) Charge/discharge profiles of  $\text{Fe}_2(\text{MoO}_4)_3$  based thin film cell at 1 C (with Na as counter electrode). Reproduced with permission.<sup>[80]</sup> Copyright 2012, Elsevier. c) Voltage profiles of  $\text{Na}_2\text{TiFe}(\text{PO}_4)_3$  and  $\text{Na}_2\text{TiCr}(\text{PO}_4)_3$ . Reproduced with permission.<sup>[79]</sup> Copyright 2003, American Chemical Society.

$\text{NaVPO}_4\text{F}$ ,  $\text{Fe}_2(\text{MoO}_4)_3$ ,  $\text{Na}_{1.5}\text{VOPO}_4\text{F}_{0.5}$ ,  $\text{Na}_3(\text{VO}_{1-x}\text{PO}_4)_2\text{F}_{1+2x}$  ( $0 \leq x \leq 1$ ),  $\text{Na}_2\text{TiFe}(\text{PO}_4)_3$ ,  $\text{Na}_3\text{Fe}_2(\text{PO}_4)_3$ , and  $\text{NaNbFe}(\text{PO}_4)_3$  etc.<sup>[78,80,185–192]</sup> For instance,  $\text{Na}_3(\text{VO}_{1-x}\text{PO}_4)_2\text{F}_{1+2x}$  ( $0 \leq x \leq 1$ ) composites were prepared via a novel solvothermal low-temperature (60–120 °C) method, delivering high capacities (110 mAh g<sup>-1</sup> when  $x = 1$ ; 112 mAh g<sup>-1</sup> when  $x = 0$ ) and good cycling performances (high capacity retentions of 93.6% and 93.8% after 200 cycles at 0.2 C, respectively).<sup>[191]</sup> Disappointingly,  $\text{Na}_3\text{Fe}_2(\text{PO}_4)_3$  was demonstrated to show low sodium accommodation capability, delivering only 45 mAh g<sup>-1</sup>.<sup>[193]</sup> Other transition metal (Mn, Ni, Cu, etc.) phosphates are facing similar problems.<sup>[7,79]</sup>

Let us address the more electro-active NASICON compounds such as  $\text{Fe}_2(\text{MoO}_4)_3$ , which is of monoclinic ( $P2_1/c$ ) crystal structure consisting of  $\text{FeO}_6$  octahedra and  $\text{MoO}_4$  tetrahedra interconnected through corner sharing oxygen atoms. It has been shown to be a promising cathode material for both Li and Na,<sup>[80,194–198]</sup> not at least due to good thermal and structural stability. The structure is shown in the insert of Figure 11a. Two  $\text{FeO}_6$  octahedra connect three  $\text{MoO}_4$  tetrahedra, forming an open tunnel and enabling a robust structure.<sup>[190]</sup> Typical charge/discharge profiles are presented in Figure 11a with a specific capacity of 95.3 mAh g<sup>-1</sup>, and two discharge plateaus at 2.55 V and 2.62 V, corresponding to subsequent insertion of two sodium ions.<sup>[80]</sup> To improve the electrochemical performance of  $\text{Fe}_2(\text{MoO}_4)_3$ , particle size reduction was undertaken by Fu et al.<sup>[185]</sup> Moreover, graphene coating was also shown to improve the electrochemical performances.<sup>[195,199]</sup> In addition, NASICON compounds with dual transition metals, such as  $\text{Na}_2\text{TiM}(\text{PO}_4)_3$  ( $M = \text{Fe}, \text{Cr}$ ) are also sodium-active

compounds corresponding to  $\text{Ti}^{3+}/\text{Ti}^{4+}$ ,  $\text{Fe}^{2+}/^{3+}$ , and  $\text{Cr}^{2+}/\text{Cr}^{3+}$  redox processes. Atomic structure and charge/discharge profiles of  $\text{Na}_2\text{TiM}(\text{PO}_4)_3$  crystals are shown in Figure 11c.<sup>[79]</sup> Two desodiation steps are involved in the redox processes for  $M = \text{Fe}, \text{Cr}$ , the first related to  $\text{Fe}^{2+}/\text{Fe}^{3+}$  and  $\text{Cr}^{2+}/\text{Cr}^{3+}$  value changes and the second to  $\text{Ti}^{3+}/\text{Ti}^{4+}$ . Albeit these NASICON materials have good thermal stability and high ionic conductivity, they need further optimization to achieve better electrochemical performances.

All relevant parameters and figures of merits for the discussed NASICON cathode materials are listed in Table 2.

### 2.3. NASICON Anode Materials

As far as SIBs anodic materials are concerned, the use of sodium metal is problematic because of safety reasons. Sodium metal is chemically more reactive than lithium and can, as Li, form dendrites during the charge/discharge process. Moreover, Na exhibits a low melting point (97.7 °C). These issues make systematic research on anode materials necessary. For any electrode, one has to distinguish between four types of storage mechanisms, viz. single phase absorption, phase-transition, conversion reaction and interfacial storage, realized in relevant materials as Na-alloys, covalent as well as ionically bonded materials, which is similar to LIB.<sup>[59,93,200–205]</sup> Owing to the usually lower solubility of Na, multi-phase reactions are of greater importance than for Li-based batteries. Unlike transitional metal oxide/sulfides involving conversion reactions, NASICON type materials such as  $\text{NaTi}_2(\text{PO}_4)_3$  (NTP),  $\text{Na}_3\text{V}_2(\text{PO}_4)_3$  and

**Table 2.** Comparison of NVP, NVPF and  $\text{Fe}_2(\text{MoO}_4)_3$  in terms of storage properties.

Materials	Morphology	Size (nm)	Capacities (mAh g <sup>-1</sup> )	Cycle number	Capacity retention	Ref.
$\text{Na}_3\text{V}_2(\text{PO}_4)_3@C$	Nanoparticles	40	104.3, at 0.5 C	50	99.6%	[131]
$\text{Na}_3\text{V}_2(\text{PO}_4)_3@C$	3D nanofibers	20–80	110, at 10 C	1000	95.9%	[122]
$\text{Na}_3\text{V}_2(\text{PO}_4)_3\text{-F/C}$	Nanofibers	10	103, at 0.1 C	50	99.3%	[125]
$\text{Na}_3\text{V}_2(\text{PO}_4)_3\text{-CS}$	Core-sheath nanowires	20–50	94, at 1C	50	74%	[133]
$C@Na_3\text{V}_2(\text{PO}_4)_3@pC$	Double-shell nanospheres	20–40	103, at 10 C	1000	80.5%	[123]
$\text{Na}_3\text{V}_2(\text{PO}_4)_3@AC$	Nanoparticles	5	100.6, at 5 C	200	96.4%	[137]
$\text{Na}_3\text{V}_2(\text{PO}_4)_3@\text{MCNT}$	MCNT nanocomposites	100	146.5, at 0.1 C	50	94.3%	[124]
$\text{Na}_3\text{V}_2(\text{PO}_4)_3@C@rGO$	3D porous composites	50	115, at 1 C; 86, at 100 C	10,000	64%	[145]
$\text{Na}_3\text{V}_2(\text{PO}_4)_3@C/G$	3D porous composites	100	86.5, at 40 C	1500	80%	[108]
$\text{Na}_3\text{V}_2(\text{PO}_4)_3@C@CMK-3$	3D CMK-3	3	115, at 1 C; 109, at 5 C	2000	68%	[121]
$\text{Na}_3\text{V}_2(\text{PO}_4)_3@\text{CNT-G}$	3D continuous free-standing foam	50–100	109, at 30 C; 82, at 100 C	2000	96%	[81]
$\text{Na}_3\text{V}_2(\text{PO}_4)_3@C\text{-N142}$	Porous particles	200	101.9, at 0.2 C	50	95.5%	[128]
$\text{Na}_3\text{V}_2(\text{PO}_4)_3@\text{C-N-CNT}$	Nanoparticles with CNT	100	93.8, at 0.2 C	400	92.2%	[129]
$\text{Na}_3\text{V}_2(\text{PO}_4)_3@\text{C-B-0.38}$	Nanoparticles	100–800	87.1, at 0.2 C	50	81%	[110]
$\text{Na}_3\text{V}_2(\text{PO}_4)_2\text{F}_3@C$	Nanorods	200	126, at 0.1 C	50	92%	[171]
$\text{Na}_3\text{V}_2(\text{PO}_4)_2\text{F}_3@\text{AC}$	Nanoparticles	40–200	116, at ≈0.1 C	50	97.6%	[183]
$\text{Na}_3\text{V}_2(\text{PO}_4)_2\text{F}_3@\text{AC}$	Porous nanoparticles	50	130, at 0.5 C	50	95%	[184]
$\text{Na}_3\text{V}_2(\text{PO}_4)_2\text{F}_3@\text{PC}$	Porous nanoparticles	<1000	111, at 1.82 C	90	98.2%	[178]
$\text{Na}_3\text{V}_2(\text{PO}_4)_2\text{F}_3/\text{PC}$	Nanoparticles	<500	111.5, at 0.091 C	100	93%	[172]
$\text{Fe}_2(\text{MoO}_4)_3$	Thin film	200	94, at 1 C	100	80.8%	[80]

$\text{NaZr}_2(\text{PO}_4)_3$  (NZP), are considered as most promising anodes for SIB with high rate capabilities. For instance, composites of  $\text{Na}_3\text{V}_2(\text{PO}_4)_3$  with rGO-CNT networks were applied as anode materials for SIB by Zhu et al. in ref. [206]. A fully 1.7 V battery delivered a reversible capacity of 90  $\text{mAh g}^{-1}$  at 10 C and achieved a capacity retention ratio of 77%.<sup>[81]</sup> In this section, we mainly discuss the preparation, property, and performance of NTP, NZP and related NASICON type materials as negative electrodes.

### 2.3.1. $\text{NaTi}_2(\text{PO}_4)_3$ (NTP)

NTP, an often use SIB anode material,<sup>[70,207,208]</sup> is a triclinic NASICON variant ( $\overline{P}1$ ), as represented by in Figure 12a.<sup>[209]</sup>

NTP reveals two discharge plateaus (at 2.1 V and 0.4 V; between 0 V and 3 V) based on  $\text{Ti}^{4+}/\text{Ti}^{3+}$  and  $\text{Ti}^{3+}/\text{Ti}^{2+}$  valence changes (as shown in Figure 12b). Within the range of 0 V and 3 V, the theoretical capacity is 200  $\text{mAh g}^{-1}$ . The discharge transforms  $\text{Na}_3\text{Ti}_2(\text{PO}_4)_3$  into  $\text{NaTi}_2(\text{PO}_4)_3$  by removing the Na atom on  $\text{Na}_2$ -sites while  $\text{Na}_2$ -sites remain unaffected.

As NVP, NTP particles suffer from insufficient electrical conductivity, the aforementioned strategy using conductive agents, such as graphene, CMK-3 and carbon shell, is useful here as well. The same is true as far as the strategy of particle size reduction is concerned. Wu et al. prepared, by a hydrothermal method,<sup>[69]</sup> 3D graphene networks embedding NTP nanoparticles (NTP@GN). Here, porous NTP nanoparticles ( $\approx 100$  nm) are homogenously distributed within the graphene nanonetwork, as shown in Figure 12c and 12d, enabling fast charge transfer and transport

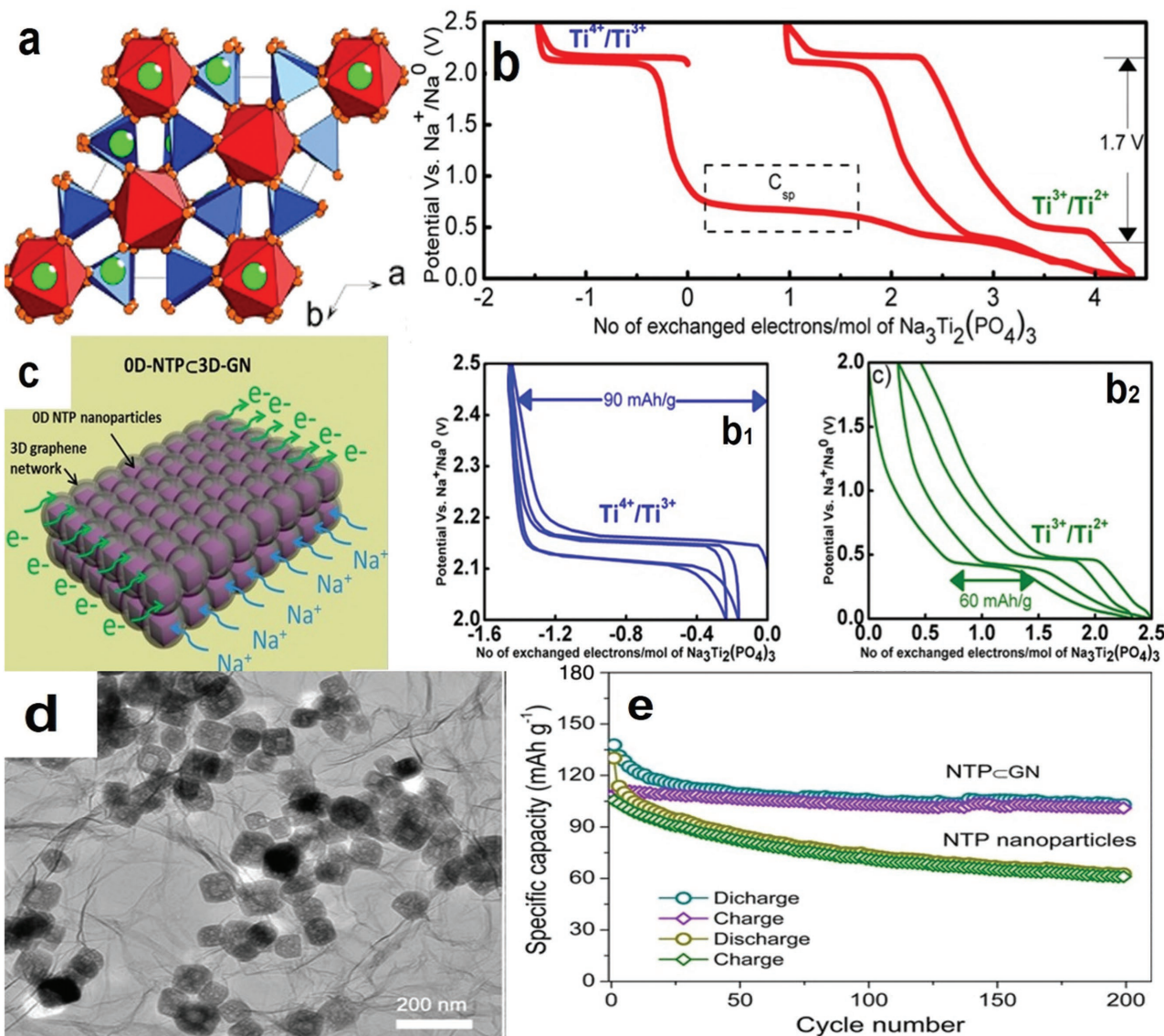


**Figure 12.** a) Triclinic structure of  $\text{Na}_3\text{Ti}_2(\text{PO}_4)_3$ . Voltage profiles of  $\text{Na}_3\text{Ti}_2(\text{PO}_4)_3$  vs  $\text{Na}^+$  between 0 V and 2.5 V (b) cycling results at higher voltage (b1, 2.0–2.5 V) and lower voltage (b2, 0–2.0 V). Reproduced with permission.<sup>[209]</sup> Copyright 2013, American Chemical Society. c) Scheme of 0D NTP nanoparticles embedded in 3D graphene networks. d) TEM image of NTP@GN. e) Cycling performance of NTP@GN. Reproduced with permission.<sup>[69]</sup> Copyright 2015, American Chemical Society.

which is maintained during cycling. NTP@GN composites (theoretical capacity of 132.8 mAh g<sup>-1</sup>), delivered a high capacity of 109 mAh g<sup>-1</sup> between 1.5 V and 3 V and good capacity retention ratio of 93% after 200 cycles as shown in Figure 12e. Another example is reported by Zhang et al. using CMK-3 as matrix. These NTP nanoparticles ( $\approx$ 5 nm) are uniformly dispersed in CMK-3 channels.<sup>[210]</sup> The obtained NTP@CMK-3 composites delivered a reversible capacity of 100 mAh g<sup>-1</sup> at 0.2 C between 1.5 V and 3 V and good cycling performance.

Wang et al. synthesized carbon-coated NVP (NTP@C) using citric acid and titanium isopropoxide as carbon source and titanium source.<sup>[112]</sup> The resulting NTP@C composites exhibit a thin carbon layer ( $\approx$ 7 nm) and the NTP nanoparticles good crystallinity. The NTP@C composites enable a high capacity of 220 mAh g<sup>-1</sup> to 82 mAh g<sup>-1</sup> at current rates of 0.1 C to 20 C with gradually increased cell polarization (0–3 V). The charge-voltage curves reveal two discharge/charge plateaus corresponding to the aforementioned two redox reactions of Ti.

### 2.3.2. $\text{NaZr}_2(\text{PO}_4)_3$ (NZP)

Another interesting NASICON-type anode material,  $\text{NaZr}_2(\text{PO}_4)_3$ , was synthesized by Jiao et al. using a one-step solid reaction method, and electrochemically investigated.<sup>[211]</sup>  $\text{NaZr}_2(\text{PO}_4)_3$  is composed of  $[\text{PO}_4]$  tetrahedra and  $[\text{ZrO}_6]$  octahedra with channels arranged by  $\text{ZrO}_6$  that host the  $\text{Na}^+$  ions

(Figure 13a). Again, the open structure allows fast motion of the  $\text{Na}^+$  ions through  $\text{PO}_4\text{-ZrO}_6$  polyhedra tunnels. The phase transitions of  $\text{NaZr}_2(\text{PO}_4)_3$  induced by variation of the Na-content is confirmed by ex situ XRD patterns (Figure 13a), demonstrating the different phase states of  $\text{Na}_2\text{Zr}_2(\text{PO}_4)_3$  (Figure 13a<sub>1</sub>) and  $\text{NaZr}_2(\text{PO}_4)_3$  (Figure 13a<sub>2</sub>) during (dis)charge processes. HRTEM image shows the two lattice spacings of 4.40 Å and 6.33 Å (Figure 13b and c), corresponding to the (110) and (012) planes. The charge/discharge profiles of NZP are shown in Figure 13d, referring to the redox reactions converting  $\text{Na}_{1-x}\text{Zr}_2(\text{PO}_4)_3$  into  $\text{Na}_{3-y}\text{Zr}_2(\text{PO}_4)_3$  ( $0 < x < 1$ ,  $0 < y < 1$ ). According to Jiao et al.,<sup>[211]</sup> the NZP compounds delivered a high capacity of 150 mAh g<sup>-1</sup> and stable Coulombic efficiency for at least 100 cycles (Figure 13e), showing the relevance of NZP as anode materials for SIB with fast kinetics and stable cycling performance.

### 2.3.3. Other NASICON Anode Materials

Most anode materials are non-Na materials such as amorphous carbon, Sb, Sn or P, requiring pre-sodiation for activation in full batteries.<sup>[179,180,212]</sup> This consumes a large amount of sodium (stemming from the cathode) to form stable SEI layers, and causes pronounced irreversible capacity losses. NASICON-type anodes are not burdened with this problem. Besides  $\text{NaTi}_2(\text{PO}_4)_3$  and  $\text{NaZr}_2(\text{PO}_4)_3$ , there are further

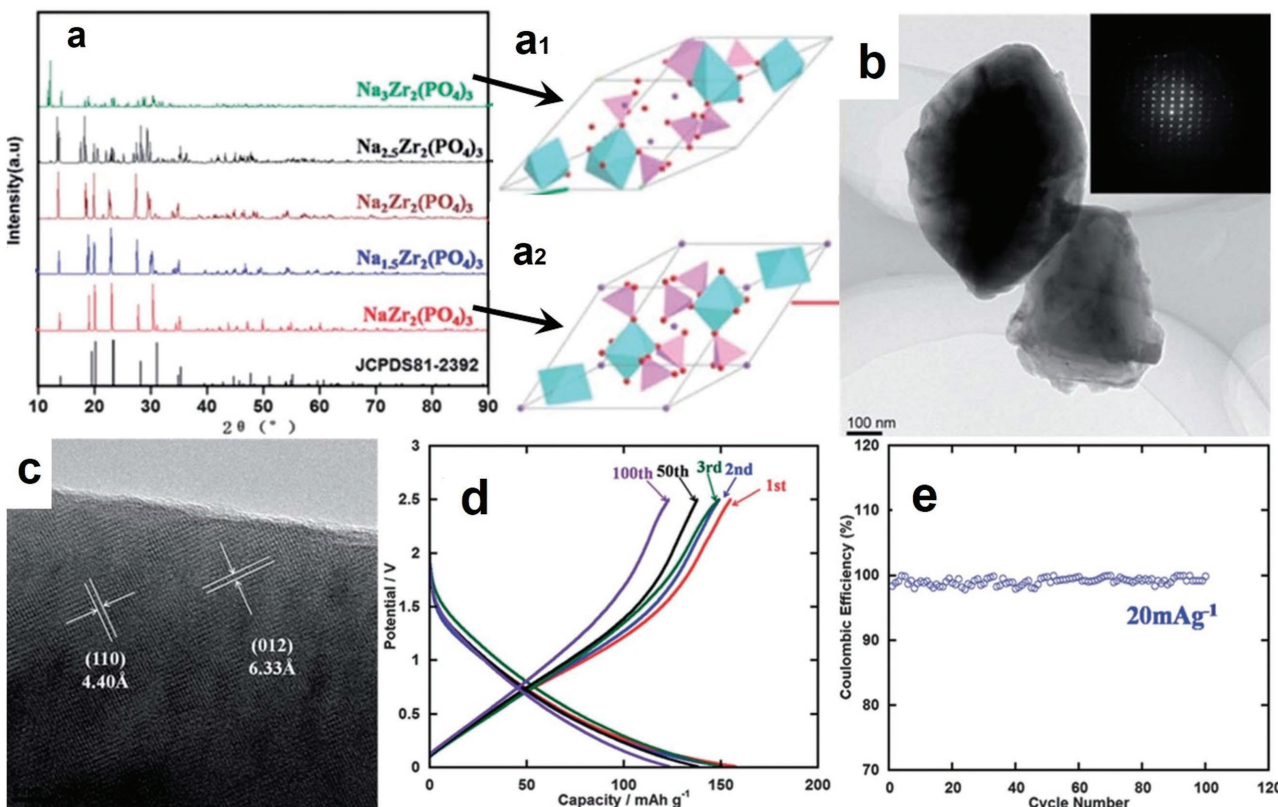


**Figure 13.** a) XRD pattern of  $\text{Na}_x\text{Zr}_2(\text{PO}_4)_3$  at different charge stages including crystal structures of  $\text{Na}_3\text{Zr}_2(\text{PO}_4)_3$  and  $\text{NaZr}_2(\text{PO}_4)_3$ . b, c) TEM and HRTEM images of  $\text{NaZr}_2(\text{PO}_4)_3$  particles. d, e) Voltage-profiles in 1<sup>st</sup>, 10<sup>th</sup> and 50<sup>th</sup> cycles and cycling performance at 20 mA g<sup>-1</sup>. Reproduced with permission.<sup>[211]</sup> Copyright 2014, Royal Society of Chemistry.

NASICON anode materials that are worthy of mention, such as  $\text{NaV}_2(\text{PO}_4)_3$ ,  $\text{Na}_3\text{V}_2(\text{PO}_4)_3$ ,  $\text{NaSn}_2(\text{PO}_4)_3$ ,  $\text{Na}_3\text{Ti}_2(\text{PO}_4)_3$ , and  $\text{Na}_3\text{MnTi}(\text{PO}_4)_3$ . For instance,  $\text{NaV}_2(\text{PO}_4)_3$  materials performed well as anode material in non-aqueous electrolyte.<sup>[81,174,213–216]</sup> Moreover,  $\text{Na}_3\text{V}_2(\text{PO}_4)_3$  is demonstrated by Jian et al. as anode materials for SIB with deep sodiation processes by the formation of  $\text{Na}_4\text{V}_2(\text{PO}_4)_3$  and  $\text{Na}_5\text{V}_2(\text{PO}_4)_3$  at 1.6 V and 0.3 V, respectively, delivering a high reversible capacity of 149 mAh g<sup>-1</sup> at 11.7 mA g<sup>-1</sup> (0.1 C) and good rate capacities.<sup>[217]</sup> Additionally,  $\text{NaSn}_2(\text{PO}_4)_3$  is illustrated as anode materials for LIB with Li foil as counter electrode by the valence changes of  $\text{Sn}^{4+}/\text{Sn}$  by the formation of Li salt as inactive matrix, demonstrating a high capacity of 320 mAh g<sup>-1</sup> at 50 mA g<sup>-1</sup> and good capacity retention of 87% as well as remarkable rate capacities up to 270 mAh g<sup>-1</sup> at 2 A g<sup>-1</sup>.<sup>[107]</sup>

The aforementioned anode materials can be also applied to assemble full cells solely based on NASICON-type electrodes, as shown in Figure 14a.<sup>[218]</sup> To give an example,  $\text{NaTi}_2(\text{PO}_4)_3$  and  $\text{Na}_3\text{V}_2(\text{PO}_4)_3$  are assembled to a full cell using an aqueous electrolyte (1 M  $\text{Na}_2\text{SO}_4$  aqueous solution), delivering an over-potential of 1.3 V and the voltage-profiles shown in

Figure 14b. In addition, the polarization gap of  $\text{NaTi}_2(\text{PO}_4)_3$  in aqueous electrolyte (2 M  $\text{Na}_2\text{SO}_4$  aqueous electrolyte) is much smaller than that in typical organic electrolytes, as shown in Figure 14c and 14d. Another typical example of NASICON full cell is reported by Goodenough et al., using  $\text{Na}_3\text{MnTi}(\text{PO}_4)_3$  as both anode and cathode in aqueous electrolyte, shown in Figure 14e.<sup>[219]</sup> The quasi-symmetric reactions are based on the redox couples of  $\text{Mn}^{3+}/\text{Mn}^{2+}$  (as cathode: reversibly extracting one sodium ion) and  $\text{Ti}^{4+}/\text{Ti}^{3+}$  (as anode: reversibly inserting one sodium ion), and the charge/discharge profiles are centered around 1.4 V without apparent polarization during cycles and characterized by a reversible capacity of 57.9 mAh g<sup>-1</sup> at 0.5 C. Moreover, the symmetric aqueous full cell exhibits exceptional rate capacities for currents ranging from 0.5 C to 10 C. Many other NASICON compositions with Mn, Ni, Ti etc. are tried by Hu et al. and the details are shown in previous report.<sup>[7]</sup>

All relevant parameters and figures of merits for the discussed anode materials are listed in Table 3.

Even more interesting is the recently reported cell by Masquelier's group, in which NVP anode and cathode are

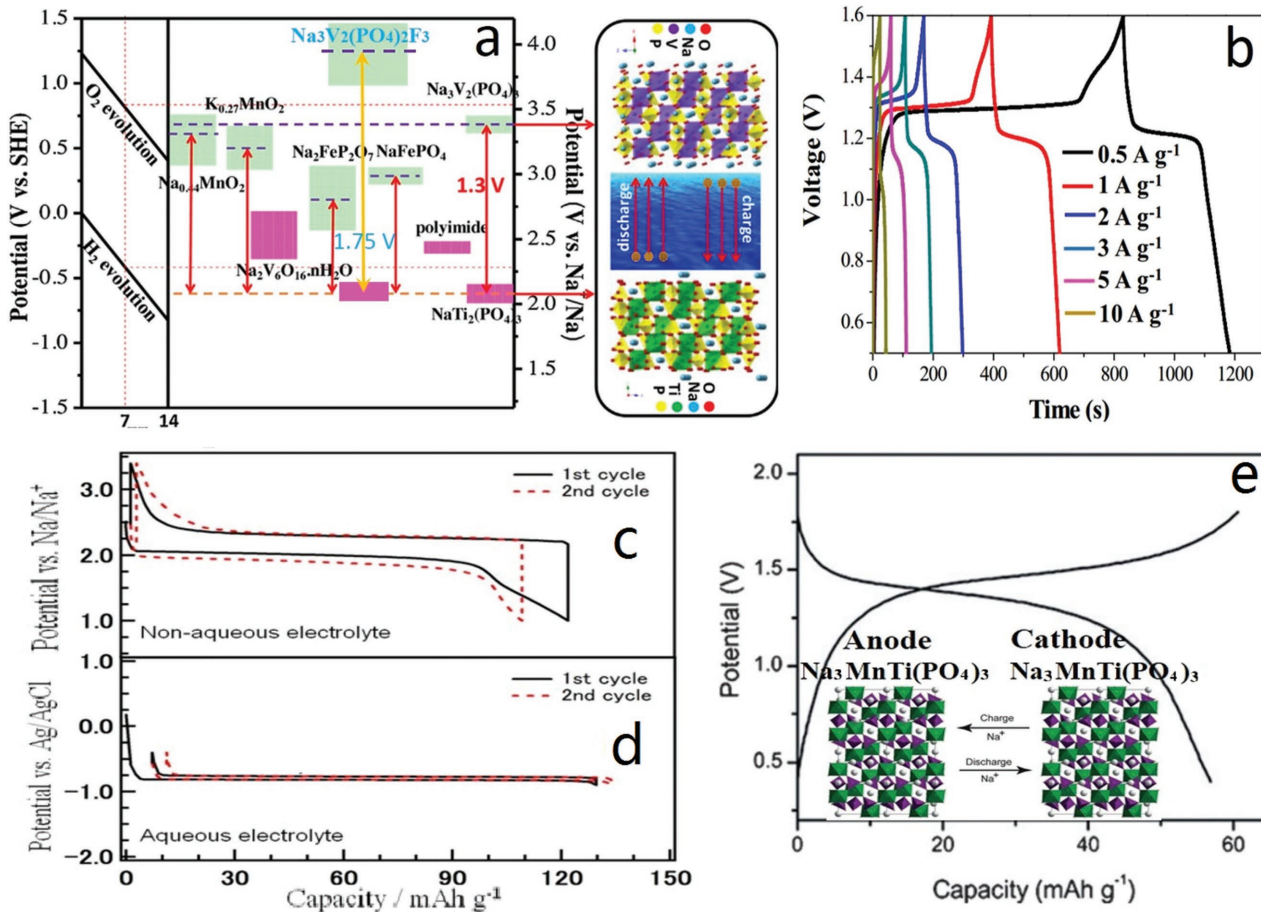


**Figure 14.** a) Working potentials and schematic structures of  $\text{NaTi}_2(\text{PO}_4)_3$  and  $\text{Na}_3\text{V}_2(\text{PO}_4)_3$  in comparison of other electrode materials. b) Voltage profiles of full cell ( $\text{NaTi}_2(\text{PO}_4)_3$  and  $\text{Na}_3\text{V}_2(\text{PO}_4)_3$  with a mass ratio of 8:7 between 0.5 V and 1.6 V). Reproduced with permission.<sup>[218]</sup> Copyright 2016, Elsevier. c, d) Charge/discharge profiles of  $\text{NaTi}_2(\text{PO}_4)_3/\text{Na}$  (non-aqueous) and  $\text{NaTi}_2(\text{PO}_4)_3/\text{Zn}$  (aqueous) at a rate of 2 mA cm<sup>-2</sup>. Reproduced with permission.<sup>[207]</sup> Copyright 2011, American Chemical Society. e) Charge/discharge profile of the symmetric full cell of  $\text{Na}_3\text{MnTi}(\text{PO}_4)_3$  and the corresponding structures at 0.5 C.

**Table 3.** Comparison of NTP, NZP, NVP, NaSn<sub>2</sub>(PO<sub>4</sub>)<sub>3</sub> and Na<sub>3</sub>MnTi(PO<sub>4</sub>)<sub>3</sub> in terms of storage properties.

Materials	Morphology	Size (nm)	Capacities (mAh g <sup>-1</sup> )	Cycle number	Capacity retention	Ref.
NaTi <sub>2</sub> (PO <sub>4</sub> ) <sub>3</sub> @graphene nanosheets	3D networks; porous nanoparticles	100	109	200	93%	[69]
NaTi <sub>2</sub> (PO <sub>4</sub> ) <sub>3</sub> @CMK-3 composites	CMK-3; nanoparticles	≈3	101	200	73%	[210]
NaTi <sub>2</sub> (PO <sub>4</sub> ) <sub>3</sub> @C composites	Thin carbon layer coated nanoparticles	≈7	220 (cycled 0 V to 3 V)	10000 (at 20 C)	68%	[112]
NaTi <sub>2</sub> (PO <sub>4</sub> ) <sub>3</sub> @graphene	2D structure with particles	100–200	104.4 (at 2 C; aqueous)	100	95.7%	[70]
NaTi <sub>2</sub> (PO <sub>4</sub> ) <sub>3</sub> @graphene	3D networks with particles	30–40	128.6 (at 0.1 C)	1000 (at 10 C)	95.5%	[221]
Na <sub>3</sub> Zr <sub>2</sub> (PO <sub>4</sub> ) <sub>3</sub>	Particles	400–500	150 (at 20 mA g <sup>-1</sup> )	100	88%	[211]
Na <sub>3</sub> V <sub>2</sub> (PO <sub>4</sub> ) <sub>3</sub> /C composites	Particles	>1000	146 (at 11.7 mA g <sup>-1</sup> )	50	91%	[217]
NaSn <sub>2</sub> (PO <sub>4</sub> ) <sub>3</sub> /C composites	Carbon coated nanoparticles	≈100	320 (at 50 mA g <sup>-1</sup> )	120	87%	[107]
Na <sub>3</sub> MnTi(PO <sub>4</sub> ) <sub>3</sub> /C composites	Random particles (aqueous)	≈30	57.9 (at 0.5 C; 29.4 mA g <sup>-1</sup> )	100 (1 C)	98%	[219]

separated by a NASICON solid electrolyte.<sup>[206,220]</sup> In this way, an all-solid-state cell solely based on NASICON structure was fabricated. Nonetheless, elevated temperature was necessary for a reasonable performance, highlighting the general difficulty of all-solid-state batteries.

### 3. Conclusions

NASICON-type materials have impressive features of stable structural framework, high ionic conductivity, and good thermal stability, which can be applied in many fields, including electrodes for both lithium ion batteries and sodium-ion batteries, solid electrolytes, membrane for lithium oxygen batteries, fuel cells and gas sensors. In the past decade, great progress has been made in the development of NASICON-type electrode materials to achieve high-performance SIBs. This review presented advantages and disadvantages of NASICON-type electrode materials, and highlighted design principles to optimize their functions. As the morphology is crucial, synthesis and electrochemical properties are intimately interlinked. The NASICON system offers a very versatile and useful platform for consistent reliable and well-working cathode and anode. At the moment, all the discussed materials exhibit specific short-comings, but various possibilities to overcome them are within the range of vision.

As far as the high average working potentials of NASICON-type materials as anode, the energy density of sodium ion full batteries shows no advantage to LIB due to lower potential gaps, which might be a stumbling block for practical application. However, this awkward situation can be enhanced by using of other anode materials with features of lower discharge potential. Compared to other sodium/lithium based cathode, NASICON-type active materials are more power oriented materials than energy oriented materials due to the high ionic conductivity and relatively low energy density. As the high ionic conductivity of NASICON materials enables very powerful Na-electrolytes, all NASICON-based all-solid-state batteries are in reach and under development in various labs.

### Acknowledgements

This work was financially supported by the National Key Research Program of China (No. 2016YFB0100305), the Sofja Kovalevskaja award and postdoctoral scholarship of the Alexander von Humboldt Foundation, by the National Natural Science Foundation of China (No. 51622210, No. 21373195), the Fundamental Research Funds for the Central Universities (WK3430000004), the Collaborative Innovation Center of Suzhou Nano Science and Technology.

### Conflict of Interest

The authors declare no conflict of interest.

### Keywords

electrode materials, NASICON-type materials, sodium-ion batteries

Received: January 21, 2017

Revised: March 2, 2017

Published online: June 19, 2017

- [1] K. Kang, Y. S. Meng, J. Bréger, C. P. Grey, G. Ceder, *Science* **2006**, 311, 977.
- [2] M. Armand, J. M. Tarascon, *Nature* **2008**, 451, 652.
- [3] W. Sun, Y. Wang, *Nanoscale* **2014**.
- [4] V. Etacheri, R. Marom, R. Elazari, G. Salitra, D. Aurbach, *Energy Environ. Sci.* **2011**, 4, 3243.
- [5] N. A. Kaskhedikar, J. Maier, *Adv. Mater.* **2009**, 21, 2664.
- [6] B. Scrosati, J. Garche, *J. Power Sources* **2010**, 195, 2419.
- [7] H. Pan, Y.-S. Hu, L. Chen, *Energy Environ. Sci.* **2013**, 6, 2338.
- [8] J. B. Goodenough, K.-S. Park, J. Am. Chem. Soc. **2013**, 135, 1167.
- [9] R. Malini, U. Uma, T. Sheela, M. Ganeshan, N. G. Renganathan, *Ionics* **2009**, 15, 301.
- [10] P. G. Bruce, B. Scrosati, J. M. Tarascon, *Angew. Chem. Int. Ed. Engl.* **2008**, 47, 2930.
- [11] S. Chen, L. Shen, P. A. v. Aken, J. Maier, Y. Yu, *Adv. Mater.* **2017**, <https://doi.org/10.1002/adma.201605650>.
- [12] L. Fu, K. Tang, K. Song, P. A. van Aken, Y. Yu, J. Maier, *Nanoscale* **2014**, 6, 1384.

- [13] M. D. Slater, D. Kim, E. Lee, C. S. Johnson, *Adv. Funct. Mater.* **2013**, *23*, 947.
- [14] W. Li, S.-L. Chou, J.-Z. Wang, J. H. Kim, H.-K. Liu, S.-X. Dou, *Adv. Mater.* **2014**, *26*, 4037.
- [15] X. Xie, D. Su, S. Chen, J. Zhang, S. Dou, G. Wang, *Chem. Asian J.* **2014**, *9*, 1611.
- [16] Y. Wen, K. He, Y. Zhu, F. Han, Y. Xu, I. Matsuda, Y. Ishii, J. Cumings, C. Wang, *Nat. Commun.* **2014**, *5*, 4033.
- [17] D. Y. W. Yu, P. V. Prikhodchenko, C. W. Mason, S. K. Batabyal, J. Gun, S. Sladkevich, A. G. Medvedev, O. Lev, *Nat. Commun.* **2013**, *4*, 2922.
- [18] S. P. Ong, V. L. Chevrier, G. Hautier, A. Jain, C. Moore, S. Kim, X. Ma, G. Ceder, *Energy Environ. Sci.* **2011**, *4*, 3680.
- [19] D. Morgan, G. Ceder, Saïdi, J. Barker, J. Swoyer, H. Huang, G. Adamson, *Chem. Mater.* **2002**, *14*, 4684.
- [20] C. Wu, P. Kopold, P. A. van Aken, J. Maier, Y. Yu, *Adv. Mater.* **2016**, n/a.
- [21] C. Zhu, X. Mu, P. A. van Aken, Y. Yu, J. Maier, *Angew. Chem. Int. Ed.* **2014**, *53*, 2152.
- [22] N. Yabuuchi, M. Kajiyama, J. Iwatate, H. Nishikawa, S. Hitomi, R. Okuyama, R. Usui, Y. Yamada, S. Komaba, *Nat. Mater.* **2012**, *11*, 512.
- [23] A. Ponrouch, E. Marchante, M. Courty, J.-M. Tarascon, M. R. Palacin, *Energy Environ. Sci.* **2012**, *5*, 8572.
- [24] S.-W. Kim, D.-H. Seo, X. Ma, G. Ceder, K. Kang, *Adv. Energy Mater.* **2012**, *2*, 710.
- [25] D. Su, G. Wang, *ACS Nano* **2013**, *7*, 11218.
- [26] S. Guo, P. Liu, H. Yu, Y. Zhu, M. Chen, M. Ishida, H. Zhou, *Angew. Chem. Int. Ed.* **2015**, *54*, 5894.
- [27] R. Berthelot, D. Carlier, C. Delmas, *Nat. Mater.* **2011**, *10*, 74.
- [28] X. Wang, G. Liu, T. Iwao, M. Okubo, A. Yamada, *J. Phys. Chem. C* **2014**, *118*, 2970.
- [29] N. Yabuuchi, M. Yano, H. Yoshida, S. Kuze, S. Komaba, *J. Electrochem. Soc.* **2013**, *160*, A3131.
- [30] C. Deng, S. Zhang, B. Zhao, *Energy Storage Mater.* **2016**, *4*, 71.
- [31] V. Palomares, P. Serras, I. Villaluenga, K. B. Hueso, J. Carretero-Gonzalez, T. Rojo, *Energy Environ. Sci.* **2012**, *5*, 5884.
- [32] H. Kabbour, D. Coillot, M. Colmont, C. Masquelier, O. Mentré, *J. Am. Chem. Soc.* **2011**, *133*, 11900.
- [33] C. Masquelier, L. Croguennec, *Chem. Rev.* **2013**, *113*, 6552.
- [34] Y. Ono, Y. Yui, M. Hayashi, K. Asakura, H. Kitabayashi, K. I. Takahashi, *ECS Trans.* **2014**, *58*, 33.
- [35] J. Pickardt, W. Paulus, M. Schmalz, R. Schöllhorn, *J. Solid State Chem.* **1990**, *89*, 308.
- [36] Y. Ono, Y. Yui, K. Asakura, J. Nakamura, M. Hayashi, K. I. Takahashi, *Am. J. Phys. Chem.* **2014**, *3*, 61.
- [37] I. Hasa, J. Hassoun, Y.-K. Sun, B. Scrosati, *ChemPhysChem* **2014**, *15*, 2152.
- [38] N. Yabuuchi, M. Kajiyama, J. Iwatate, H. Nishikawa, S. Hitomi, R. Okuyama, R. Usui, Y. Yamada, S. Komaba, *Nat. Mater.* **2012**, *11*, 512.
- [39] Y. Cao, L. Xiao, W. Wang, D. Choi, Z. Nie, J. Yu, L. V. Saraf, Z. Yang, J. Liu, *Adv. Mater.* **2011**, *23*, 3155.
- [40] H. Liu, H. Zhou, L. Chen, Z. Tang, W. Yang, *J. Power Sources* **2011**, *196*, 814.
- [41] Z. Jian, Y.-S. Hu, X. Ji, W. Chen, *Adv. Mater.* **2017**, n/a.
- [42] S. Komaba, Y. Matsuura, T. Ishikawa, N. Yabuuchi, W. Murata, S. Kuze, *Electrochim. Commun.* **2012**, *21*, 65.
- [43] M. He, K. Kravchyk, M. Walter, M. V. Kovalenko, *Nano Lett.* **2014**, *14*, 1255.
- [44] B. Farbod, K. Cui, W. P. Kalisvaart, M. Kupsta, B. Zahiri, A. Kohandehghan, E. M. Lotfabad, Z. Li, E. J. Luber, D. Mitlin, *ACS Nano* **2014**, *8*, 4415.
- [45] L. Baggetto, J. K. Keum, J. F. Browning, G. M. Veith, *Electrochim. Commun.* **2013**, *34*, 41.
- [46] P. R. Abel, M. G. Fields, A. Heller, C. B. Mullins, *ACS Appl. Mater. Interfaces* **2014**, *6*, 15860.
- [47] Y.-M. Lin, P. R. Abel, A. Gupta, J. B. Goodenough, A. Heller, C. B. Mullins, *ACS Appl. Mater. Interfaces* **2013**, *5*, 8273.
- [48] H. Zhu, Z. Jia, Y. Chen, N. Weadock, J. Wan, O. Vaaland, X. Han, T. Li, L. Hu, *Nano Lett.* **2013**, *13*, 3093.
- [49] Y. Cao, L. Xiao, M. L. Sushko, W. Wang, B. Schwenzer, J. Xiao, Z. Nie, L. V. Saraf, Z. Yang, J. Liu, *Nano Lett.* **2012**, *12*, 3783.
- [50] J.-M. Fan, J.-J. Chen, Q. Zhang, B.-B. Chen, J. Zang, M.-S. Zheng, Q.-F. Dong, *ChemSusChem* **2015**, *8*, 1856.
- [51] W. Luo, Z. Jian, Z. Xing, W. Wang, C. Bommier, M. M. Lerner, X. Ji, *ACS Cent. Sci.* **2015**, *1*, 516.
- [52] J. Sun, H.-W. Lee, M. Pasta, Y. Sun, W. Liu, Y. Li, H. R. Lee, N. Liu, Y. Cui, *Energy Storage Mater.* **2016**, *4*, 130.
- [53] J. Sun, H.-W. Lee, M. Pasta, H. Yuan, G. Zheng, Y. Sun, Y. Li, Y. Cui, *Nat. Nano* **2015**, *10*, 980.
- [54] W.-J. Li, S.-L. Chou, J.-Z. Wang, H.-K. Liu, S.-X. Dou, *Nano Lett.* **2013**, *13*, 5480.
- [55] S. Wei, S. Xu, A. Agrawal, S. Choudhury, Y. Lu, Z. Tu, L. Ma, L. A. Archer, *Nat. Commun.* **2016**, *7*, 11722.
- [56] X. Xie, S. Chen, B. Sun, C. Wang, G. Wang, *ChemSusChem* **2015**, *8*, 2948.
- [57] X. Xie, D. Su, J. Zhang, S. Chen, A. K. Mondal, G. Wang, *Nanoscale* **2015**, *7*, 3164.
- [58] J. Wang, C. Luo, T. Gao, A. Langrock, A. C. Mignerey, C. Wang, *Small* **2015**, *11*, 473.
- [59] Q. Sun, Q.-Q. Ren, H. Li, Z.-W. Fu, *Electrochim. Commun.* **2011**, *13*, 1462.
- [60] Y. Wang, D. Su, C. Wang, G. Wang, *Electrochim. Commun.* **2013**, *29*, 8.
- [61] X. Wang, S. Kajiyama, H. Iinuma, E. Hosono, S. Oro, I. Moriguchi, M. Okubo, A. Yamada, *Nat. Commun.* **2015**, *6*, 6544.
- [62] H. Xiong, M. D. Slater, M. Balasubramanian, C. S. Johnson, T. Rajh, *J. Phys. Chem. Lett.* **2011**, *2*, 2560.
- [63] X. Xie, Z. Ao, D. Su, J. Zhang, G. Wang, *Adv. Funct. Mater.* **2015**, *25*, 1393.
- [64] C. Chen, Y. Wen, X. Hu, X. Ji, M. Yan, L. Mai, P. Hu, B. Shan, Y. Huang, *Nat. Commun.* **2015**, *6*, 6929.
- [65] X. Xie, D. Su, S. Chen, J. Zhang, S. Dou, G. Wang, *Chem. — Asian J.* **2014**, *9*, 1611.
- [66] Y. Zhu, X. Han, Y. Xu, Y. Liu, S. Zheng, K. Xu, L. Hu, C. Wang, *ACS Nano* **2013**, *7*, 6378.
- [67] L. Wu, X. Hu, J. Qian, F. Pei, F. Wu, R. Mao, X. Ai, H. Yang, Y. Cao, *Energy Environ. Sci.* **2014**, *7*, 323.
- [68] J. Fullenwarth, A. Darwiche, A. Soares, B. Donnadieu, L. Monconduit, *J. Mater. Chem. A* **2014**, *2*, 2050.
- [69] C. Wu, P. Kopold, Y.-L. Ding, P. A. van Aken, J. Maier, Y. Yu, *ACS Nano* **2015**, *9*, 6610.
- [70] G. Pang, C. Yuan, P. Nie, B. Ding, J. Zhu, X. Zhang, *Nanoscale* **2014**, *6*, 6328.
- [71] X. Li, X. Zhu, J. Liang, Z. Hou, Y. Wang, N. Lin, Y. Zhu, Y. Qian, *J. Electrochim. Soc.* **2014**, *161*, A1181.
- [72] A. Manthiram, J. Choi, *J. Power Sources* **2006**, *159*, 249.
- [73] S. Li, J. Qiu, C. Lai, M. Ling, H. Zhao, S. Zhang, *Nano Energy* **2015**, *12*, 224.
- [74] M. Winter, J. O. Besenhard, M. E. Spahr, P. Novák, *Adv. Mater.* **1998**, *10*, 725.
- [75] B. Scrosati, *J. Electrochim. Soc.* **1992**, *139*, 2776.
- [76] Aluminium Foil for Battery Cathode Substrate, [www.mtixtl.com/aluminumFoilforBatteryCathodeSubstrate-EQ-bcaf15u-280.aspx](http://www.mtixtl.com/aluminumFoilforBatteryCathodeSubstrate-EQ-bcaf15u-280.aspx) (accessed: December 2016).
- [77] M. Sawicki, L. L. Shaw, *RSC Adv.* **2015**, *5*, 53129.
- [78] N. Anantharamulu, K. Koteswara Rao, G. Rambabu, B. Vijaya Kumar, V. Radha, M. Vithal, *J. Mater. Sci.* **2011**, *46*, 2821.

- [79] S. Patoux, G. Rousse, J.-B. Leriche, C. Masquelier, *Chem. Mater.* **2003**, *15*, 2084.
- [80] Q. Sun, Q.-Q. Ren, Z.-W. Fu, *Electrochem. Commun.* **2012**, *23*, 145.
- [81] C. Zhu, P. Kopold, P. A. van Aken, J. Maier, Y. Yu, *Adv. Mater.* **2016**, *28*, 2409.
- [82] W. Song, X. Ji, Z. Wu, Y. Zhu, Y. Yang, J. Chen, M. Jing, F. Li, C. E. Banks, *J. Mater. Chem. A* **2014**, *2*, 5358.
- [83] H. Y. P. Hong, *Mater. Res. Bull.* **1976**, *11*, 173.
- [84] J. B. Goodenough, H. Y. P. Hong, J. A. Kafalas, *Mater. Res. Bull.* **1976**, *11*, 203.
- [85] P. Colombari, *Solid State Ionics* **1986**, *21*, 97.
- [86] A. Clearfield, *Solid State Ionics* **1983**, *9*, 823.
- [87] H. Kohler, H. Schulz, *Mater. Res. Bull.* **1985**, 1461.
- [88] J. P. Boilot, G. Collin, R. Comes, *J. Solid State Chem.* **1983**, *50*, 91.
- [89] K.-D. Kreuer, H. Kohler, J. Maier, in *High Conductivity Solid Ionic Conductors: Recent Trends and Applications* (Ed. T. Takahashi), Singapore **1989**, pp. 242.
- [90] J. Maier, U. Warhus, *J. Chem. Thermodyn.* **1986**, *18*, 309.
- [91] J. Maier, *Solid State Ionics* **2000**, *131*, 13.
- [92] Z. Ming-sen, M. Jun, D. Quan-feng, L. Zu-geng, *Battery Bimonthly* **2007**, *37*, 199.
- [93] J. Maier, *Angew. Chem. Int. Ed.* **2013**, *52*, 4998.
- [94] J. Maier, *J. Am. Ceram. Soc.* **1993**, *76*, 1212.
- [95] J. Maier, **2005**, pp. 300.
- [96] D. J. Kim, R. Ponraj, A. G. Kannan, H.-W. Lee, R. Fathi, R. Ruffo, C. M. Mari, D. K. Kim, *J. Power Sources* **2013**, *244*, 758.
- [97] Y. Zhu, Y. Xu, Y. Liu, C. Luo, C. Wang, *Nanoscale* **2013**, *5*, 780.
- [98] S. Guo, Y. Sun, J. Yi, K. Zhu, P. Liu, Y. Zhu, G.-z. Zhu, M. Chen, M. Ishida, H. Zhou, *NPG Asia Mater.* **2016**, *8*, e266.
- [99] R. Amin, P. Balaya, J. Maier, *Electrochem. Solid-State Lett.* **2007**, *10*, A13.
- [100] P. P. Prosini, M. Lisi, D. Zane, M. Pasquali, *Solid State Ionics* **2002**, *148*, 45.
- [101] M. W. Verbrugge, B. J. Koch, *J. Electrochem. Soc.* **1996**, *143*, 600.
- [102] P. Yu, B. N. Popov, J. A. Ritter, R. E. White, *J. Electrochem. Soc.* **1999**, *146*, 8.
- [103] M. Kühne, F. Paolucci, J. Popovic, P. M. Ostrovsky, J. Maier, J. H. Smet, *ARXIV* **2017**, 1.
- [104] X. H. Rui, N. Yesibolati, S. R. Li, C. C. Yuan, C. H. Chen, *Solid State Ionics* **2011**, *187*, 58.
- [105] E. de la Llave, V. Borgel, K.-J. Park, J.-Y. Hwang, Y.-K. Sun, P. Hartmann, F.-F. Chesneau, D. Aurbach, *ACS Appl. Mater. Interfaces* **2016**, *8*, 1867.
- [106] D. H. Lee, J. Xu, Y. S. Meng, *Phys. Chem. Chem. Phys.* **2013**, *15*, 3304.
- [107] P. Hu, J. Ma, T. Wang, B. Qin, C. Zhang, C. Shang, J. Zhao, G. Cui, *Chem. Mater.* **2015**, *27*, 6668.
- [108] J. Fang, S. Wang, Z. Li, H. Chen, L. Xia, L. Ding, H. Wang, *J. Mater. Chem. A* **2016**, *4*, 1180.
- [109] N. Böckenfeld, A. Balducci, *J. Solid State Electrochem.* **2014**, *18*, 959.
- [110] W. Shen, H. Li, C. Wang, Z. Li, Q. Xu, H. Liu, Y. Wang, *J. Mater. Chem. A* **2015**, *3*, 15190.
- [111] Y. Niu, M. Xu, Y. Zhang, J. Han, Y. Wang, C. M. Li, *RSC Adv.* **2016**, *6*, 45605.
- [112] D. Wang, Q. Liu, C. Chen, M. Li, X. Meng, X. Bie, Y. Wei, Y. Huang, F. Du, C. Wang, G. Chen, *ACS Appl. Mater. Interfaces* **2016**, *8*, 2238.
- [113] F. Sagane, *J. Electrochem. Soc.* **2016**, *163*, A2835.
- [114] S. Song, H. M. Duong, A. M. Korsunsky, N. Hu, L. Lu, *Sci. Rep.* **2016**, *6*, 32330.
- [115] J.-Y. Shin, D. Samuelis, J. Maier, *Adv. Funct. Mater.* **2011**, *21*, 3464.
- [116] S. Y. Lim, H. Kim, R. A. Shakoob, Y. Jung, J. W. Choi, *J. Electrochem. Soc.* **2012**, *159*, A1393.
- [117] K. M. Bui, V. A. Dinh, S. Okada, T. Ohno, *Phys. Chem. Chem. Phys.* **2015**, *17*, 30433.
- [118] Z. Jian, C. Yuan, W. Han, X. Lu, L. Gu, X. Xi, Y.-S. Hu, H. Li, W. Chen, D. Chen, Y. Ikuhara, L. Chen, *Adv. Funct. Mater.* **2014**, *24*, 4265.
- [119] W. Song, X. Cao, Z. Wu, J. Chen, K. Huangfu, X. Wang, Y. Huang, X. Ji, *Phys. Chem. Chem. Phys.* **2014**, *16*, 17681.
- [120] Z. Jian, W. Han, X. Lu, H. Yang, Y.-S. Hu, J. Zhou, Z. Zhou, J. Li, W. Chen, D. Chen, L. Chen, *Adv. Energy Mater.* **2013**, *3*, 156.
- [121] Y. Jiang, Z. Yang, W. Li, L. Zeng, F. Pan, M. Wang, X. Wei, G. Hu, L. Gu, Y. Yu, *Adv. Energy Mater.* **2015**, *5*, 1402104.
- [122] W. Ren, Z. Zheng, C. Xu, C. Niu, Q. Wei, Q. An, K. Zhao, M. Yan, M. Qin, L. Mai, *Nano Energy* **2016**, *25*, 145.
- [123] C. Zhu, K. Song, P. A. van Aken, J. Maier, Y. Yu, *Nano Lett.* **2014**, *14*, 2175.
- [124] M. Chen, K. Kou, M. Tu, J. Hu, B. Yang, *Solid State Ionics* **2015**, *274*, 24.
- [125] J. Liu, K. Tang, K. Song, P. A. van Aken, Y. Yu, J. Maier, *Nanoscale* **2014**, *6*, 5081.
- [126] Q. Zhang, W. Wang, Y. Wang, P. Feng, K. Wang, S. Cheng, K. Jiang, *Nano Energy* **2016**, *20*, 11.
- [127] Z. Jian, L. Zhao, H. Pan, Y.-S. Hu, H. Li, W. Chen, L. Chen, *Electrochem. Commun.* **2012**, *14*, 86.
- [128] W. Shen, C. Wang, Q. Xu, H. Liu, Y. Wang, *Adv. Energy Mater.* **2015**, *5*, 1400982.
- [129] W. Shen, H. Li, Z. Guo, C. Wang, Z. Li, Q. Xu, H. Liu, Y. Wang, Y. Xia, *ACS Appl. Mater. Interfaces* **2016**, *8*, 15341.
- [130] X. Zhu, Y. Fang, X. Ai, H. Yang, Y. Cao, *J. Alloy. Compd.* **2015**, *646*, 170.
- [131] W. Duan, Z. Zhu, H. Li, Z. Hu, K. Zhang, F. Cheng, J. Chen, *J. Mater. Chem. A* **2014**, *2*, 8668.
- [132] H. Li, Y. Bai, F. Wu, Q. Ni, C. Wu, *Solid State Ionics* **2015**, *278*, 281.
- [133] S. Kajiyama, J. Kikkawa, J. Hoshino, M. Okubo, E. Hosono, *Chem. Eur. J.* **2014**, *20*, 12636.
- [134] J. Kang, S. Baek, V. Mathew, J. Gim, J. Song, H. Park, E. Chae, A. K. Rai, J. Kim, *J. Mater. Chem.* **2012**, *22*, 20857.
- [135] Y. Zhai, Y. Dou, D. Zhao, P. F. Fulvio, R. T. Mayes, S. Dai, *Adv. Mater.* **2011**, *23*, 4828.
- [136] D.-W. Wang, Q. Zeng, G. Zhou, L. Yin, F. Li, H.-M. Cheng, I. R. Gentle, G. Q.M. Lu, *J. Mater. Chem. A* **2013**, *1*, 9382.
- [137] S. Li, Y. Dong, L. Xu, X. Xu, L. He, L. Mai, *Adv. Mater.* **2014**, *26*, 3545.
- [138] D. C. Elias, R. R. Nair, T. M.G. Mohiuddin, S. V. Morozov, P. Blake, M. P. Halsall, A. C. Ferrari, D. W. Boukhvalov, M. I. Katsnelson, A. K. Geim, K. S. Novoselov, *Science* **2009**, *323*, 610.
- [139] S. Chen, W. Yeoh, Q. Liu, G. Wang, *Carbon* **2012**, *50*, 4557.
- [140] S. Chen, Y. Wang, H. Ahn, G. Wang, *J. Power Sources* **2012**, *216*, 22.
- [141] B. Zhan, C. Li, J. Yang, G. Jenkins, W. Huang, X. Dong, *Small* **2014**, *10*, 4042.
- [142] L. Liao, J. Zhu, X. Bian, L. Zhu, M. D. Scanlon, H. H. Girault, B. Liu, *Adv. Funct. Mater.* **2013**, *23*, 5326.
- [143] R. Raccichini, A. Varzi, S. Passerini, B. Scrosati, *Nat Mater.* **2015**, *14*, 271.
- [144] R. Raccichini, A. Varzi, D. Wei, S. Passerini, *Adv. Mater.* **2016**.
- [145] X. Rui, W. Sun, C. Wu, Y. Yu, Q. Yan, *Adv. Mater.* **2015**, *27*, 6670.
- [146] D. Gu, H. Bongard, Y. Deng, D. Feng, Z. Wu, Y. Fang, J. Mao, B. Tu, F. Schüth, D. Zhao, *Adv. Mater.* **2010**, *22*, 833.
- [147] J. Wang, W. Li, F. Wang, Y. Xia, A. M. Asiri, D. Zhao, *Nanoscale* **2014**, *6*, 3217.
- [148] S. Chen, X. Huang, B. Sun, J. Zhang, H. Liu, G. Wang, *J. Mater. Chem. A* **2014**.
- [149] J. Schuster, G. He, B. Mandlmeier, T. Yim, K. T. Lee, T. Bein, L. F. Nazar, *Angew. Chem. Int. Ed.* **2012**, *51*, 3591.
- [150] J. Sforzini, P. Hapala, M. Franke, G. van Straaten, A. Stöhr, S. Link, S. Soubatch, P. Jelínek, T. L. Lee, U. Starke, M. Švec, F. C. Bocquet, F. S. Tautz, *Phy. Rev. Lett.* **2016**, *116*, 126805.

- [151] Y. Lin, S. Wu, W. Shi, B. Zhang, J. Wang, Y. A. Kim, M. Endo, D. S. Su, *Chem. Commun.* **2015**, *51*, 13086.
- [152] X. Xie, D. Su, J. Zhang, S. Chen, A. K. Mondal, G. Wang, *Nanoscale* **2015**, *7*, 3164.
- [153] K. Cui, S. Hu, Y. Li, *Electrochim. Acta* **2016**, *210*, 45.
- [154] J.-Z. Guo, X.-L. Wu, F. Wan, J. Wang, X.-H. Zhang, R.-S. Wang, *Chem. Eur. J.* **2015**, *21*, 17371.
- [155] H. Wang, T. Maiyalagan, X. Wang, *ACS Catal.* **2012**, *2*, 781.
- [156] J. Sforzini, P. Hapala, M. Franke, G. van Straaten, A. Stöhr, S. Link, S. Soubatch, P. Jelínek, T. L. Lee, U. Starke, M. Švec, F. C. Bocquet, F. S. Tautz, *Phys. Rev. Lett.* **2016**, *116*, 126805.
- [157] H. Fei, J. Dong, M. J. Arellano-Jiménez, G. Ye, N. Dong Kim, E. L.G. Samuel, Z. Peng, Z. Zhu, F. Qin, J. Bao, M. J. Yacaman, P. M. Ajayan, D. Chen, J. M. Tour, *Nat. Commun.* **2015**, *6*, 8668.
- [158] F. Joucken, Y. Tison, P. Le Fèvre, A. Tejeda, A. Taleb-Ibrahimi, E. Conrad, V. Repain, C. Chacon, A. Bellec, Y. Girard, S. Rousset, J. Ghijssen, R. Sporken, H. Amara, F. Ducastelle, J. Lagoute, *Sci. Rep.* **2015**, *5*, 14564.
- [159] Y. Shao, S. Zhang, M. H. Engelhard, G. Li, G. Shao, Y. Wang, J. Liu, I. A. Aksay, Y. Lin, *J. Mater. Chem.* **2010**, *20*, 7491.
- [160] D. Zahn, P. Heitjans, J. Maier, *Chem. Eur. J.* **2012**, *18*, 6225.
- [161] H.-W. Liang, W. Wei, Z.-S. Wu, X. Feng, K. Müllen, *J. Am. Chem. Soc.* **2013**, *135*, 16002.
- [162] T. Chen, L. Pan, T. A.J. Loh, D. H.C. Chua, Y. Yao, Q. Chen, D. Li, W. Qin, Z. Sun, *Dalton Trans.* **2014**, *43*, 14931.
- [163] L. G. Bulusheva, A. V. Okotrub, A. G. Kurenya, H. Zhang, H. Zhang, X. Chen, H. Song, *Carbon* **2011**, *49*, 4013.
- [164] B. Kuchta, L. Firlej, S. Roszak, P. Pfeifer, *Adsorption* **2010**, *16*, 413.
- [165] Z.-S. Wu, W. Ren, L. Xu, F. Li, H.-M. Cheng, *ACS Nano* **2011**, *5*, 5463.
- [166] J. Han, L. L. Zhang, S. Lee, J. Oh, K.-S. Lee, J. R. Potts, J. Ji, X. Zhao, R. S. Ruoff, S. Park, *ACS Nano* **2013**, *7*, 19.
- [167] D.-Y. Yeom, W. Jeon, N. D.K. Tu, S. Y. Yeo, S.-S. Lee, B. J. Sung, H. Chang, J. A. Lim, H. Kim, *Sci. Rep.* **2015**, *5*, 9817.
- [168] K. Xia, H. Zhan, Y. Wei, Y. Gu, *Beilstein J. Nanotechnol.* **2014**, *5*, 329.
- [169] Y. Lin, Y. Zhu, B. Zhang, Y. A. Kim, M. Endo, D. S. Su, *J. Mater. Chem. A* **2015**, *3*, 21805.
- [170] R. A. Shakoor, D.-H. Seo, H. Kim, Y.-U. Park, J. Kim, S.-W. Kim, H. Gwon, S. Lee, K. Kang, *J. Mater. Chem.* **2012**, *22*, 20535.
- [171] J. Geng, F. Li, S. Ma, J. Xiao, M. Sui, *Int. J. Electrochem. Sci.* **2016**, *11*, 3815.
- [172] W. Song, X. Ji, Z. Wu, Y. Zhu, F. Li, Y. Yao, C. E. Banks, *RSC Adv.* **2014**, *4*, 11375.
- [173] Z. Liu, Y.-Y. Hu, M. T. Dunstan, H. Huo, X. Hao, H. Zou, G. Zhong, Y. Yang, C. P. Grey, *Chem. Mater.* **2014**, *26*, 2513.
- [174] M. Bianchini, F. Fauth, N. Brisset, F. Weill, E. Suard, C. Masquelier, L. Croguennec, *Chem. Mater.* **2015**, *27*, 3009.
- [175] K. Chihara, A. Kitajou, I. D. Gocheva, S. Okada, J.-i. Yamaki, *J. Power Sources* **2013**, *227*, 80.
- [176] W. Song, Z. Wu, J. Chen, Q. Lan, Y. Zhu, Y. Yang, C. Pan, H. Hou, M. Jing, X. Ji, *Electrochim. Acta* **2014**, *146*, 142.
- [177] Q. Liu, X. Meng, Z. Wei, D. Wang, Y. Gao, Y. Wei, F. Du, G. Chen, *ACS Appl. Mater. Interfaces* **2016**, *8*, 31709.
- [178] W. Song, X. Ji, J. Chen, Z. Wu, Y. Zhu, K. Ye, H. Hou, M. Jing, C. E. Banks, *Phys. Chem. Chem. Phys.* **2015**, *17*, 159.
- [179] B. Zhang, R. Dugas, G. Rousse, P. Rozier, A. M. Abakumov, J.-M. Tarascon, *Nat. Commun.* **2016**, *7*, 10308.
- [180] H. Wang, Y. Xiao, C. Sun, C. Lai, X. Ai, *RSC Adv.* **2015**, *5*, 106519.
- [181] M. Kohl, F. Borrmann, H. Althues, S. Kaskel, *Adv. Energy Mater.* **2016**, *6*, 1502185.
- [182] A. Moretti, M. Secchiaroli, D. Buchholz, G. Giuli, R. Marassi, S. Passerini, *J. Electrochem. Soc.* **2015**, *162*, A2723.
- [183] W. Song, X. Ji, Z. Wu, Y. Yang, Z. Zhou, F. Li, Q. Chen, C. E. Banks, *J. Power Sources* **2014**, *256*, 258.
- [184] Q. Liu, D. Wang, X. Yang, N. Chen, C. Wang, X. Bie, Y. Wei, G. Chen, F. Du, *J. Mater. Chem. A* **2015**, *3*, 21478.
- [185] V. T. Nguyen, Y. L. Liu, S. A. Hakim, S. Y. Amr Rady Radwan, W. Chen, *Int. J. Electrochem. Sci.* **2015**, *10*, 10565.
- [186] F. Sauvage, E. Quarez, J. M. Tarascon, E. Baudrin, *Solid State Sci.* **2006**, *8*, 1215.
- [187] R. Essehli, I. Belharouak, H. Ben Yahia, K. Maher, A. Abouimrane, B. Orayech, S. Calder, X. L. Zhou, Z. Zhou, Y. K. Sun, *Dalton Trans.* **2015**, *44*, 7881.
- [188] J. Isasi, A. Daidouh, *Solid State Ionics* **2000**, *133*, 303.
- [189] M. Xu, C.-J. Cheng, Q.-Q. Sun, S.-J. Bao, Y.-B. Niu, H. He, Y. Li, J. Song, *RSC Adv.* **2015**, *5*, 40065.
- [190] S. Zhou, G. Barim, B. J. Morgan, B. C. Melot, R. L. Brutcher, *Chem. Mater.* **2016**, *28*, 4492.
- [191] Y. Qi, L. Mu, J. Zhao, Y.-S. Hu, H. Liu, S. Dai, *Angew. Chem. Int. Ed.* **2015**, *54*, 9911.
- [192] J. Zhao, L. Mu, Y. Qi, Y.-S. Hu, H. Liu, S. Dai, *Chem. Commun.* **2015**, *51*, 7160.
- [193] C. Masquelier, C. Wurm, J. Rodríguez-Carvajal, J. Gaubicher, L. Nazar, *Chem. Mater.* **2000**, *12*, 525.
- [194] D. Li, J. Xue, M. Liu, *New J. Chem.* **2015**, *39*, 1910.
- [195] Y. Niu, M. Xu, J. Alloy. Compd. **2016**, *674*, 392.
- [196] Y. Song, H. Wang, Z. Li, N. Ye, L. Wang, Y. Liu, *RSC Adv.* **2015**, *5*, 16386.
- [197] V. Nguyen, Y. Liu, Y. Li, S. A. Hakim, X. Yang, W. Chen, *ECS J. Solid State Sci. Technol.* **2015**, *4*, M25.
- [198] V. Nguyen, Y. Liu, X. Yang, W. Chen, *ECS Electrochem. Lett.* **2015**, *4*, A29.
- [199] J. Sheng, H. Zang, C. Tang, Q. An, Q. Wei, G. Zhang, L. Chen, C. Peng, L. Mai, *Nano Energy* **2016**, *24*, 130.
- [200] S. Chen, Z. Ao, B. Sun, X. Xie, G. Wang, *Energy Storage Mater.* **2016**, *5*, 180.
- [201] J. Park, J.-S. Kim, J.-W. Park, T.-H. Nam, K.-W. Kim, J.-H. Ahn, G. Wang, H.-J. Ahn, *Electrochim Acta* **2013**, *92*, 427.
- [202] X. Xie, K. Kretschmer, J. Zhang, B. Sun, D. Su, G. Wang, *Nano Energy* **2015**, *13*, 208.
- [203] Y. Kim, K.-H. Ha, S. M. Oh, K. T. Lee, *Chem. Eur. J.* **2014**, *20*, 11980.
- [204] S. Hariharan, K. Saravanan, P. Balaya, *Electrochem. Commun.* **2013**, *31*, 5.
- [205] M. R. Palacin, *Chem. Soc. Rev.* **2009**, *38*, 2565.
- [206] F. Lalère, J. B. Leriche, M. Courty, S. Boulineau, V. Viallet, C. Masquelier, V. Seznec, *J. Power Sources* **2014**, *247*, 975.
- [207] S. I. Park, I. Gocheva, S. Okada, J.-i. Yamaki, *J. Electrochem. Soc.* **2011**, *158*, A1067.
- [208] Y. Fang, L. Xiao, J. Qian, Y. Cao, X. Ai, Y. Huang, H. Yang, *Adv. Energy Mater.* **2016**, *6*, 1502197.
- [209] P. Senguttuvan, G. Rousse, M. E. Arroyo y de Dompablo, H. Vezin, J. M. Tarascon, M. R. Palacin, *J. Am. Chem. Soc.* **2013**, *135*, 3897.
- [210] G. Pang, P. Nie, C. Yuan, L. Shen, X. Zhang, H. Li, C. Zhang, *J. Mater. Chem. A* **2014**, *2*, 20659.
- [211] W. Wang, B. Jiang, L. Hu, S. Jiao, *J. Mater. Chem. A* **2014**, *2*, 1341.
- [212] I. Hasa, S. Passerini, J. Hassoun, *RSC Adv.* **2015**, *5*, 48928.
- [213] Y. Zhang, H. Zhao, Y. Du, *J. Mater. Chem. A* **2016**, *4*, 7155.
- [214] G. B. Xu, L. W. Yang, X. L. Wei, J. W. Ding, J. X. Zhong, P. K. Chu, *J. Power Sources* **2016**, *327*, 580.
- [215] Z. Huang, L. Liu, L. Yi, W. Xiao, M. Li, Q. Zhou, G. Guo, X. Chen, H. Shu, X. Yang, X. Wang, *J. Power Sources* **2016**, *325*, 474.
- [216] Y. Niu, M. Xu, C. Guo, C. M. Li, *J. Colloid Interf. Sci.* **2016**, *474*, 88.
- [217] Z. Jian, Y. Sun, X. Ji, *Chem. Commun.* **2015**, *51*, 6381.
- [218] Q. Zhang, C. Liao, T. Zhai, H. Li, *Electrochim Acta* **2016**, *196*, 470.
- [219] H. Gao, J. B. Goodenough, *Angew. Chem. Int. Ed.* **2016**, *55*, 12768.
- [220] C. Masquelier, *Nat. Mater.* **2011**, *10*, 649.
- [221] H.-K. Roh, H.-K. Kim, M.-S. Kim, D.-H. Kim, K. Y. Chung, K. C. Roh, K.-B. Kim, *Nano Res.* **2016**, *9*, 1844.